Archives of Civil and Mechanical Engineering (2025) 25:86
https://doi.org/10.1007/s43452-025-01117-6

ORIGINAL ARTICLE

Application of optimized spring–mass–damper pedestrian load models for vibration assessment of footbridges: numerical and experimental investigation of a cable-stayed system

Chiara Bedon[1] · **Izabela Joanna Drygala**[2] · **Joanna Maria Dulinska**[2] · **Dorota Jasińska**[2]

Received: 31 July 2024 / Revised: 3 December 2024 / Accepted: 8 January 2025

Abstract
This article explores the potential and accuracy of spring–mass–damper (SMD) pedestrian load modelling strategies for assessing human-induced vibrations of in-service footbridges. To this aim, a recent SMD modelling proposal based on uncoupled single-body measures (SMD-0, in the following) is specifically used for the calibration of key input parameters. Finite element numerical assumptions and findings are robustly supported by original experimental tests carried out on a case-study footbridge in Poland, proving that the proposed approach can serve as an effective tool for analysing vibrations in pedestrian systems. The research study, most importantly, integrates theoretical modelling with empirical and experimental validations, to enhance the credibility of the obtained results, as well as to support the general applicability of the presented methodology. Complex in-field tests are in fact conducted on the selected footbridge, aiming to assess the effects of pedestrians on its dynamic response. Numerical analyses, which are successively performed in ABAQUS/Standard, for a set of examined walking configurations, confirm the high sensitivity of the footbridge to resonance, which was also observed during the in-field tests. The presently used SMD-0 approach is further assessed towards past SMD literature proposals. As shown, the comparison of standard structural performance indicators (such as the peak acceleration value, root mean square and CREST factor) reveals a significant sensitivity of the footbridge response to the input parameters for the analyzed SMD models. Besides, the presently addressed SMD-0 model has the advantage of being based on single-body sensor measurements and its calibration is not affected by structural features. As such, potential applications of present findings could include the improvement of design standards and safety measures for similar structures.

Keywords Vibration serviceability · Human-induced vibrations · Footbridges · Dynamic analysis · Spring–mass–damper (SMD) walking model · Human–structure interaction (HSI)

1 Introduction

As known, the unique feature of footbridges, i.e., their low mass relative to their span, significantly affects their dynamic behavior. Unlike traditional bridges, footbridges have a unique impact on, and interaction with pedestrians [1]. As footbridge users spend more time there, compared to those traveling by car across a bridge, they are more directly affected by the structures' dynamic behavior, hence potentially experiencing discomfort [2]. Moreover, pedestrians walking across the footbridge represent themselves a source of dynamic loading, and an additional influencing parameter [3]. In general, civil engineering consistently faces the challenge of providing high levels of comfort for individuals [4], ensuring acceptable structural functionality in the presence of vibrations [5], and developing effective real-time

✉ Izabela Joanna Drygala
izabela.drygala@pk.edu.pl

Chiara Bedon
chiara.bedon@dia.units.it

Joanna Maria Dulinska
joanna.dulinska@pk.edu.pl

Dorota Jasińska
dorota.jasinska@pk.edu.pl

[1] University of Trieste, Piazzale Europa 1, 34127 Trieste, Italy

[2] Cracow University of Technology, Warszawska 24, 31-155 Krakow, Poland

Published online: 12 February 2025

vibration measurement techniques [6]. Therefore, particular attention is necessary, especially during the design phase of footbridges, to ensure they possess appropriate characteristics [7] to avoid such situations like the (in)famous Millenium Bridge problem in London, in 2000 [8].

The dynamic features and performances of footbridges are significantly influenced by their low natural vibration frequencies [3]. Many historic [9] and modern [10] footbridges have natural frequencies that align closely with the critical frequencies of dynamic forces generated by walking pedestrians. This alignment can lead to major resonance phenomena [11], which are particularly noticeable in slender and lightweight pedestrian bridges. As a result, over the past few decades, there has been a substantial increase in research aimed at comprehending and enhancing the dynamic performance of footbridges [12]. Literature research, in this regard, has covered various aspects, including examining dynamic response to human-induced loads [13] and aerodynamic effects [14], optimization aspects of material usage [15], the structure monitoring technique [16], the validation of numerical simulations against measured dynamic properties [17] and the assessment of their resistance to seismic activity [18].

In general, footbridge users generate dynamic loading during three main types of activities: walking, running, and jumping [19]. Based on case studies from recent design projects, several observations can be made regarding the dynamic properties of footbridges [20]. Specifically, possible loading scenarios for footbridges can be categorized into five critical cases: (1) single-user loading; (2) spatially unrestricted pedestrian movement, representing normal pedestrian traffic; (3) spatially restricted pedestrian movement, representing crowd loading; (4) group loading, which depicts a cluster of users moving in close proximity to each other; (5) vandal loading, where a user or group of users attempt to excite the structure by moving in a harmonized, correlated manner within areas sensitive to dynamic responses. In this paper load cases 1 and 3 are covered with maximum number pf pedestrians equal to 2. For the quantification purposes of dynamic forces generated by footbridge users, two domain types of analytical models can be found in literature: time-domain and frequency-domain models [19].

Various mathematical models representing human activity loads have been proposed for time-domain analysis [19], with a predominant focus on walking. Loads resulting from human activities typically consist of static and dynamic elements, yet frequently, the dynamic component is oversimplified, inaccurately represented, or disregarded altogether [21]. This oversight can result in overly cautious design assumptions and/or unfavourable serviceability conditions, along with excessive vibrations. A straightforward method to depict the force exerted by a walking pedestrian involves employing a vertical dynamic Force Models (FM), in which human is replaced by a force, reproducing the ground reaction, fluctuating in both position and intensity over time [22].

While straightforward to apply and effective for computational purposes, these deterministic procedures have well-known limitations, since they overlook the dynamic coupling effects arising from human–structure interaction (HSI) [23]. Hence, they are accurate for certain structural configurations only, and in particular, where the dynamic interaction with pedestrian motion is minimal [24].

Therefore, a more comprehensive approach, which regards the human body as a spring–mass–damper (SMD) oscillating system, was initiated as a mathematical tool for conducting more sustainable numerical simulations aimed at addressing HSI issues [25] related to the dynamic performance of lightweight and low-damping footbridge floors [26], steel footbridges [27], as well as long-span footbridges in general [28]. These models can effectively capture the movement characteristics and impact of walkway users. Accurately quantifying these effects on structures is of paramount significance for assessing vibration serviceability often necessitating specialized computations [27]. Numerous reliable analytical methods are available in literature for calibrating SMD models, with experimental and numerical validations [29].

In structural terms, SMD biodynamic pedestrian models describe pedestrians using an equivalent mass (m) concentrated at the body's center of mass, along with a spring of stiffness (k) and a dashpot for damping coefficient (c), which interact with the supporting structure during user motion. The dynamic problem involves in fact a moving SMD model with frequency (f_m), interacting with a substructure characterized by mass (M), fundamental vibration frequency (f_1), damping ratio (ξ_s), and potential sensitivity to vibrations. In addition, even more complex biodynamic models, such as bipedal [30], considering the randomness of human walking [28] or lateral human induced vibrations [31] could be employed for advanced HSI calculations [32, 33]. However, for a broad category of footbridges with high transverse stiffness—and consequently high frequencies of lateral vibrations—the dominant vibrations are vertical. These vertical vibrations can be effectively captured by SMD models, which are suitable for the dynamic assessment of footbridges, as described in references [34] or [35]. Especially when more advanced analyses are needed, the SMD models prove invaluable. These models help quantify the HSI and its impact on the slender structure's dynamic response. Therefore, this mathematical approach can be used

for designing effective vibration control systems for pedestrian bridges. For instance, in papers [36] and [37], the SMD model was used to simulate the dynamic forces pedestrians exert on a footbridge, which were then employed to evaluate the effectiveness of the proposed tuned mass damper (TMD) in controlling the bridge's vibrations.

The main focus of the presented research is the assessment of the SMD pedestrian model recently proposed in [38], to verify its accuracy and potential use in evaluating the dynamic behaviour of footbridges. The investigation is thus conducted on a selected case study cable-stayed footbridge in Pcim (Poland), for which the modal properties [17] and seismic performance [18] have been already discussed. From past research efforts, it was recognized that the footbridges' primary natural eigenpairs fall within the typical range of dynamic loadings generated by pedestrians. The greatest sensitivity of the footbridge to pedestrian impact, was identified for vertical forces. For this reason, the structure was identified as a suitable testing ground for vertical SMD model assessment, and the research plan focused on assessing pedestrian pacing models that disregard lateral excitation effects.

The novelty and impact of the presented study lies in applying a SMD model originally developed on the base on uncoupled body-motion records, tested, and validated on floors with a single pedestrian stamping [38], to footbridges under pedestrians walking, which, to the best of the authors' knowledge, has not been previously explored.

For the presently reported research study, original in-field experimental tests were conducted for the selected footbridge in Pcim. The scheme of investigation stages is presented in Fig. 1. The main objective of the in-field experimental tests was to assess: (1) the experimental modal model of the footbridge; (2) the tension force in footbridge cables; (3) the experimental measurements of bridge responses to pedestrian traffic. Then, the numerical analysis was conducted in ABAQUS/Standard for all examined configurations in dynamic implicit simulations based on experimentally validated finite element (FE) model of the footbridge. Due to the high sensitivity to resonance observed during the in-field tests of the footbridge, the numerical investigation primarily focused on the impact of human-induced vibrations. Moreover, different pedestrian models are considered for evaluating the response of the selected footbridge, as a further assessment of the SMD proposal reported in [38].

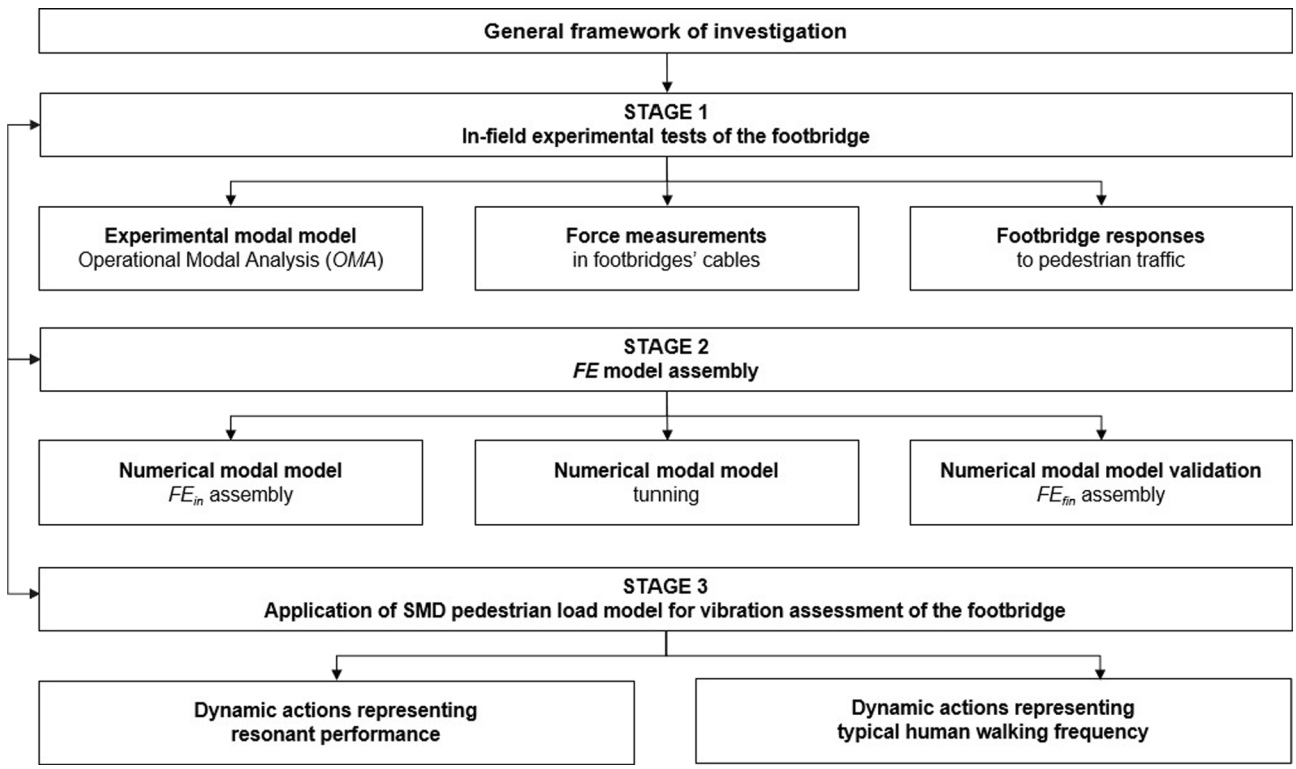

Fig. 1 Concept of the present experimental and numerical investigation

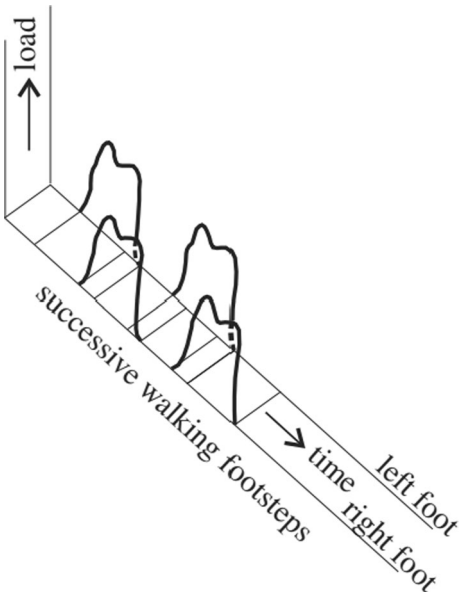

Fig. 2 3D vertical time history of the forces executed by a pedestrian for the left and right foot [39]

2 Analytical modelling of human walking—theoretical background

Mathematical models for pedestrians in the time-domain can be categorized as deterministic or probabilistic. Deterministic models aim to establish a single force formula for human walking, assuming a fixed relationship. On the other hand, probabilistic approach takes into account the variation in force–time history that individuals exhibit across repeated experiments. Figure 2 presents a 3D vertical time history of forces associated to a single pedestrian during motion (left and right foot [39]).

For the dynamic forces generated by single pedestrians walking across footbridges, deterministic time-domain mathematical models are recommended in existing design standards and guidelines for bridge engineering practice: ISO 10137:2007(E) [40], SÉTRA 2006 [41], Eurocode 1 [42], BS NA EN 1991–2 [43]. The dynamic loading is generated for longitudinal, lateral, and vertical directions, while successive walking footsteps are considered (see Fig. 2). In this study, only the vertical (V) impacts are taken into account.

For numerical simulations purposes, it is useful to assume that a pedestrian produces the dynamic force $P_V(x,t)$ that is a spatial and time varying function and can be quantified by the following equation:

$$P_V(x_i,t) = F_V(t)\big(H(x_i - vt) - H(x_i - v(t+1/f_p))\big) \quad (1)$$

where:

$F_V(t)$ is the time product of dynamic excitation for vertical direction;

H is the Heaviside function;

$x_i \in \{x_1 \dots x_n\}$ is the pedestrian position during the i th step along to the footbridge centreline;

n is the number of steps (dependent on the footbridge length and the stride length);

v is the pedestrian velocity (dependent on step frequency and the stride length);

t is the time;

f_p is the walking frequency.

The forces produced by a persons' rhythmic body motion can be represented by the Fourier series of n harmonics [21] or [41]. The time product of vertical (V) dynamic excitation $F_V(t)$ for a walking user can be expressed as follows [22]:

$$F_V(t) = G + \sum_{i=1}^{n} G\alpha_i \sin(2\pi i f_p t - \phi_i) \quad (2)$$

where:

G is the static weight of the pedestrian ([N]);

α_i is the Fourier coefficient of the i^{th} harmonic, i.e., dynamic load factor (DLF);

f_p is the walking frequency ([Hz]);

ϕ_i is the phase lag of the i^{th} harmonic to the 1^{st} harmonic;

i is the number of i^{th} harmonics;

n is the number of harmonics used in calculations.

Researchers quantify Dynamic Load Factors (DLF), which form the basis of the models, assuming perfectly periodic human-induced force. Exemplary, Blanchard et al. [20] developed a walking force model for footbridges, specifically addressing the first harmonic, assigning the DLF of 0.257 for pedestrians weighing 700 N. This model is intended for footbridges with a vertical fundamental frequency of up to 4 Hz. If the fundamental frequency falls between 4 and 5 Hz, reduction factors are applied to account for the lower amplitude of the second harmonic, as the first harmonic of walking cannot excite this frequency range. Bachmann and Ammann [21] provided DLF values for the first harmonics of the vertical force ranging between 0.4 (at a frequency of 2.0 Hz) and 0.5 (at 2.4 Hz), with linear interpolation for the intermediate frequencies. For the second and third harmonics, they suggested identical DLFs of 0.1 for pacing frequencies around 2 Hz. The Bachman model is recommended by ISO 10137:2007(E) standard [40] and SÉTRA document [41].

Another simplified mathematical approach for the time product of dynamic excitation in the vertical direction, representing the passage of pedestrians, is outlined in BS EN 1991–2:2003 (UK National Annex to EC1) [43]. Based on this standard, the vertical force in time $F_V(t)$ is formulated as follows:

$$F_V(t) = F_0 k(f_v)\sqrt{1+\gamma(N-1)}sin(2\pi f_v t) \quad (3)$$

where:

N is the number of pedestrians in the walking group (structure categorization into bridge class);

F_0 is the reference amplitude of the fluctuating force;

f_v is the natural frequency ($[Hz]$) of the vertical mode under consideration;

$k(f_v)$ is the combined population and harmonic factor;

γ is the reduction factor on effective number of pedestrians expressed as a function of effective span length (S_{eff}) and structural damping (δ);

S_{eff} is an effective span length ($[m]$), for all cases it is conservative to use $S_{eff} = S$;

S is the span of the footbridge ($[m]$).

2.1 Spring–mass–damper (SMD) biodynamic model for human walking

Biomechanics, accounting for human movement dynamic factors, such as body rotation and step length, is crucial in analysing force distribution generated by pedestrians. In footbridge design, especially for high-traffic areas with induced vibrations, biodynamic models are essential for understanding human–structure interaction (HSI). These models represent the coupled system of pedestrians and structures, aiming in addressing lightweight and low-damping footbridge behaviour. Various biodynamic models, single or multiple degree of freedom (SDOF/MDOF), simulate pedestrian vertical kinematics. These models predict individual behaviour during walking, crucial for footbridge design to ensure pedestrian comfort and safety. Efficient biodynamic models typically use spring–mass–damper (SMD) mechanisms, often formulated as single degree of freedom (SDOF) systems, capturing relative motion between the pedestrian's centre of gravity and the floor (see Fig. 3).

The fundamental assumption of the SMD biodynamic model of a walking pedestrian in the vertical direction is that the equivalent body mass m is lumped at the center of mass of a pedestrian and connected to the floor with the spring of stiffness k and a viscous damper of a coefficient c (see Fig. 3). The equivalent mass m is interpreted as a generalized parameter of the vibrating walking pedestrian body. The dynamic parameters c, and k of the model do not have a direct relationship with parts of the human body. These values are selected in a way that enables the model to reproduce or simulate accelerations that have been measured during experiments at the centre of gravity level [29].

In last decades, various multiple-degree-of-freedom biodynamic models have been developed. Miyamori et al. (2001) [44] created a three-degree-of-freedom biodynamic model to illustrate the dynamics of human walking. The authors determined the mass, stiffness, and damping parameters of the model based on observations of pedestrians crossing footbridges. They observed a slight decrease in the footbridge response when using this model compared to force models. On the other hand, Kim et al. (2008) [45] proposed a two-degree-of-freedom biodynamic model for a pedestrian walking along a footbridge. The parameters of the model were adopted from ISO 5982 [46], but for standing individuals. In contrast to the former study, the authors found that the dynamic responses of the footbridge obtained using the biodynamic model were larger than those obtained with the force model. This difference was attributed to the effects of HSI.

In later studies, a shift towards SDOF biodynamic models to represent walking pedestrians can be observed. Caprani et al. (2011) [47] investigated the vertical vibrations of a flexible, simply supported footbridge under the influence of a single pedestrian crossing it. The representation of a single individual involved either a SMD model or a traditional

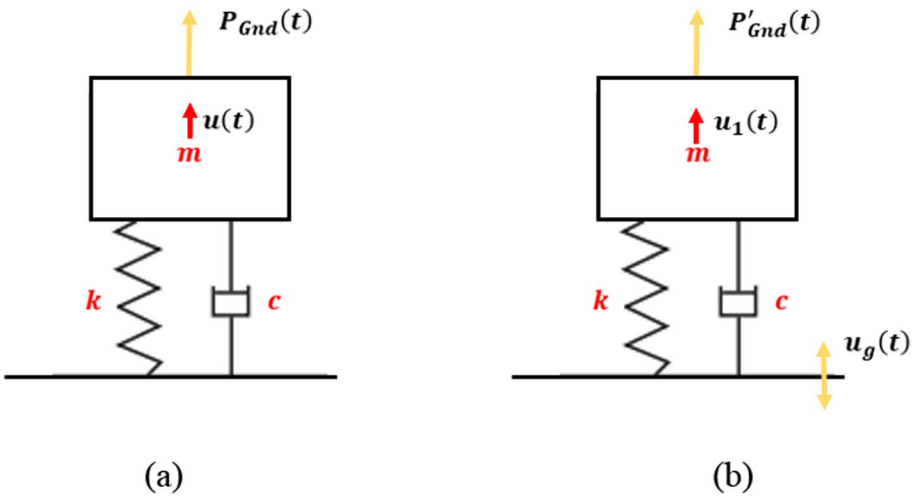

Fig. 3 Biodynamic schematic mechanical system for a walking human on (**a**) rigid or (**b**) flexible structure

moving force model. In the SMD model, the body mass of the pedestrian was considered as a generalized mass parameter, with spring stiffness and damping coefficient values derived from experimental studies done by other authors. The research revealed that when the bridge frequency matched the pacing frequency, a substantial decrease in the predicted acceleration response of the footbridge was observed when using the SMD model, compared to the response obtained from traditional moving force models. However, for bridges with frequencies slightly different from the mean, moving force models seem to be sufficient.

2.2 Literature SMD biodynamic models adopted in this study for dynamic analyses

The main objective of this paper is to compare the dynamic performance and assess the footbridge vibration under different pedestrian load models. To accomplish this objective, five literature models simulating a walking pedestrian were adopted in this work. Each model is an SDOF–SMD biodynamic model of a walking pedestrian in vertical direction, characterized by three key parameters: equivalent mass m, viscous damping coefficient c, and stiffness k.

The model developed in [38], which is used as a reference for numerical investigations and comparisons, is defined as SMD-0 in this work. To calibrate its input parameters, the body accelerations of an individual were measured by one sensor attached to the pedestrian's waist, which makes the approach particularly efficient for general purposes and applications. Experimental data from 30 random walks and more than 300 gaits on a rigid floor served for elaborating empirical expression for c, and k as a function of a pacing frequency f_p ($[Hz]$), according to Eq. 4a, b:

$$k = 8190 f_p - 4315.8 \tag{4a}$$

$$c = 7040 - 2957.5 f_p \tag{4b}$$

The equivalent mass m equals the real body mass of the pedestrian M.

The next SMD model, designated as SMD-1 in this study, was created by Silva et al. [48]. Its biodynamic parameters were derived from experimental tests involving 20 pedestrians walking along a rigid floor with accelerometers attached to their waists to record the motion of the Center of Mass (CoM). Based on these data, the following regression expressions for parameters m, c, and k were suggested for SDM-1 model (Eq. 5a, b, c):

$$m = m\left(f_p, M\right) = 97.082 + 0.275M - 32.52 f_p \tag{5a}$$

$$c = c(m) = 107.455 + 16.208m \tag{5b}$$

$$k = k(c) = 5758.441 + 11.103c \tag{5b}$$

The model developed by Toso et al. [49] is referred to as SMD-2 in this work. To obtain the biodynamic parameters of the model tests on a 6 m long force platform were performed with a set of 35 individuals walking along the platform. In the experiment, the acceleration amplitudes at the waist level and the corresponding amplitudes of the vertical ground reaction force were simultaneously registered. The measurement results were the basis for establishing the dependence of the biodynamic parameters m, c, and k on pacing frequency f_p along with the pedestrian body mass M, using regression analysis and an artificial neural network. The following expressions were finally proposed for SDM-2 model (Eq. 6a, b, c):

$$m = m\left(f_p, M\right) = -231.34 + 3.69M + 154.06 f_p - 1.97 M f_p + 0.005M^2 - 15.25 f_p^2 \tag{6a}$$

$$c = c(M, m) = -1115.69 + 92.56M - 108.94m + 2.91Mm - 1.33M^2 - 1.30m^2 \tag{6b}$$

$$k = k\left(M, f_p\right) = 75601.45 - 1295.32M - 33786.75 f_p + 506.44 M f_p + 3.59M^2 + 539.39 f_p^2 \tag{6c}$$

The determination of the biodynamic parameters for the model established by Pfeil et al. [24], further denoted as SMD-3, is based on calibration approach. The authors determined m, c, and k through experimental tests, in which 53 people were walking individually along a rigid floor and a flexible platform at three different speeds. The measurements, including the vertical ground force and the acceleration of pedestrians' waists, served to establish biodynamic parameters of the SMD-3 model. The calibration process [50] implemented for this model assumes that a decrease in the equivalent mass m occurs, and the stiffness k relates linearly to m (Eq. 7a, b):

$$m = m\left(f_p, M\right) = 0.874M - 9.142 f_p + 12.94 \tag{7a}$$

$$k = k(m) = 360.3m - 1282.5 \tag{7b}$$

The damping coefficient c must be estimated based on the iterative calculations of damping ratio (fraction of critical damping) ξ, as a function of damped frequency f_{md} of the pedestrian physical model:

$$\xi = \xi\left(f_{md}\right) = (-20.818 f_{md} + 87.513)/100 \tag{8}$$

The natural (f_m) and damped (f_{md}) frequencies of the pedestrian physical model equal:

$$f_{md} = f_m\sqrt{1-\xi^2} \tag{9a}$$

$$f_m = \sqrt{k/(4m\pi^2)} \tag{9b}$$

The last adopted model, referred to as SMD-4, was developed by Wang et al. [51]. The authors conducted experimental tests with 56 pedestrians walking on a rigid tract 40 m long and equipped with a wireless insole sensor system to measure a continuous ground reaction force induced by human walking. Based on the data transmitted to the acquisition station, with the use of the parameter identification procedure [52], the parameters of the model, and the biomechanical force were identified simultaneously in time. Under assumption that $m = M$ the authors formulated the linear dependence of natural frequency f_m and damping ratio ξ of the model on the pacing frequency f_p (Eq. 10) as follows:

$$f_m = f_m(f_p) = 0.3049f_p + 1.367 \tag{10a}$$

$$\xi = \xi(f_p) = -0.2116f_p + 0.8737 \tag{10b}$$

Having f_m, the spring stiffness k can be extracted from Eq. 9b.

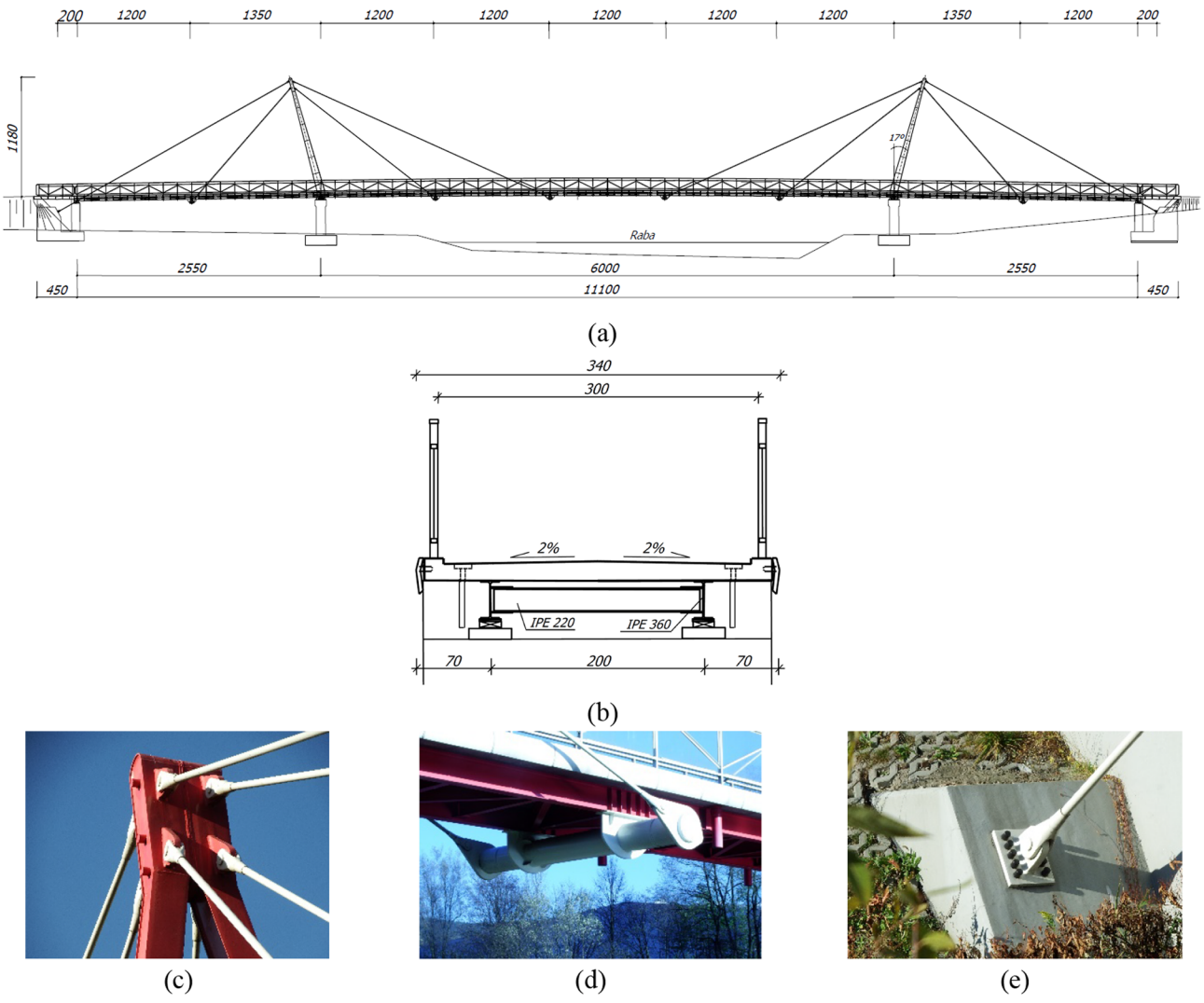

Fig. 4 Side view (**a**) and cross section (**b**) of the cable-stayed footbridge—dimensions in [mm]. Connections of cables with the structural elements of the footbridge (**c**), (**d**), (**e**)

3 Cable-stayed footbridge as a case study—structure morphology

The selected footbridge is a cable-stayed steel–concrete composite bridge with total length of 120.00 m and usable width of the deck equal to 3.00 m (see Fig. 4). It consists of three spans, with the central span measuring 60.00 m in length and the two outer spans, each 25.50 m long. The deck is constructed as a combination of steel girders and a steel-reinforced concrete slab, with the slab thickness ranging from 15.00 to 18.00 cm. The steel beams, used to form a grid structure, are made of IPE360 (for girders) and IPE220 (for cross bars). Prestressed cables connect the deck to two steel pylons, each one with 11.80 m in height (17° the inclination). The footbridge deck was suspended from steel pylons using the Macalloy 460 bar system with a diameter of 64 mm. The lengths of the cables are as follows: 1) external span: 28.00 m and 16.00 m; 2) middle span: 30.00 m and 19.00 m. Connections of cables with the other structural elements of the footbridge are shown in Fig. 4c, d and e. At main span, the suspension is designed at four points spaced every 12.00 m. The side spans is suspended at a single point located 13.50 m from the centreline of the intermediate pier. Elastomeric bearings serve as linking elements between the deck and the abutments. The pillars and abutments are supported by reinforced concrete piles with a diameter of 100 cm. The parameters of applied materials are compiled in Table 1.

4 In-field experimental tests

The configurations of measurement points for the experimental modal models of the footbridge and the experimental measurements of bridge responses to pedestrian traffic scenarios are illustrated in Fig. 5a. Each of six measurement points (A–F) was equipped in three piezoelectric high-sensitivity accelerometers (393B12 PCB Piezotronics), each capable of detecting vibrations in three directions. The frequency range of the accelerometers spanned from 0.15 to 1000 Hz. All sensors were connected via wires, and the signal was sampled at a rate of 1024 Hz. The force measurements in footbridge cables (1.1–2.8 in Fig. 5a) were made using the relationship between the vibrations of a stretched cable and a longitudinal force. The cables' free vibrations were registered based on contactless measurements and checked with the classical (accelerometer) approach. Most popular contactless methods [52] used to asses vibrations of structures or their parts are optical camera—based motion capture systems [53] and laser vibrometers [54]. In this study the RSV-150 laser Doppler vibrometer [55] (see Fig. 5) and the 356B18 triaxial accelerometer located one-quarter of the span of the stay cable were used.

Table 1 Mechanical parameters of construction materials for the examined footbridge

Material	Young Modulus $E[GPa]$	Poisson ratio $\nu[-]$	Density $\rho_m[\frac{kg}{m^3}]$
Steel (grid)	195	0.3	7850
Steel (cables)	210	0.3	7850
Concrete C25/30	31	0.2	2500

4.1 Experimental modal model of the footbridge

The modal parameters of the footbridges were assessed experimentally through measurements and analysis of vibrations induced by ambient loadings. To this aim, data from various control points were collected (refer to Fig. 5a). To estimate the natural frequencies of the experimental modal model, the cross-spectral density functions (CSD) between recorded time histories of accelerations $a_{i,j,..}(t)$ at all output measurement points and directions were determined (Eq. 11): (Fig. 6a), (Fig. 7), (see Fig. 8)

$$CSD(f) = \int_{-\infty}^{\infty} R(\tau)e^{-j2\pi ft}dt \tag{11a}$$

$$R(\tau) = \lim_{t\to\infty}\left(\frac{1}{t}\right)\int_{-\frac{t}{2}}^{\frac{t}{2}} a_i(t)a_j(t+\tau)dt \tag{11b}$$

where $R(\tau)$ is cross-corelation function between $a_i(t)$ and $a_j(t)$.

The least square complex exponential (LSCE) method was used to estimate footbridge's modal frequency and damping values. On this basis the mode shape coefficients were obtained using least square frequency domain (LSFD) method. The global experimental modal model of the footbridge was obtained (see Table 2 and Fig. 7). The analysis was assembled using LMS Test.Lab [56]. Figure 6 presents the modal model estimators, i.e., normalized summation for all combinations of auto- and cross-spectral density functions (Fig. 6a) and phase angle (Fig. 6b). The modal validation of the obtained experimental modal model was conducted based on (1) $Auto - MAC_{ij}$ matrix verification (see Fig. 8) and (2) complexity and phase scatter rating evaluation (see Table 2) (Fig. 7).

First, the $auto - MAC_{ij}$ matrix, estimating the correlation between different experimental modes, was obtained (see Fig. 8). The $auto - MAC_{ij}$ indicator is defined based on the Modal Assurance Criterion (MAC) metrics, which, in a broader context, can be extended to compare any two

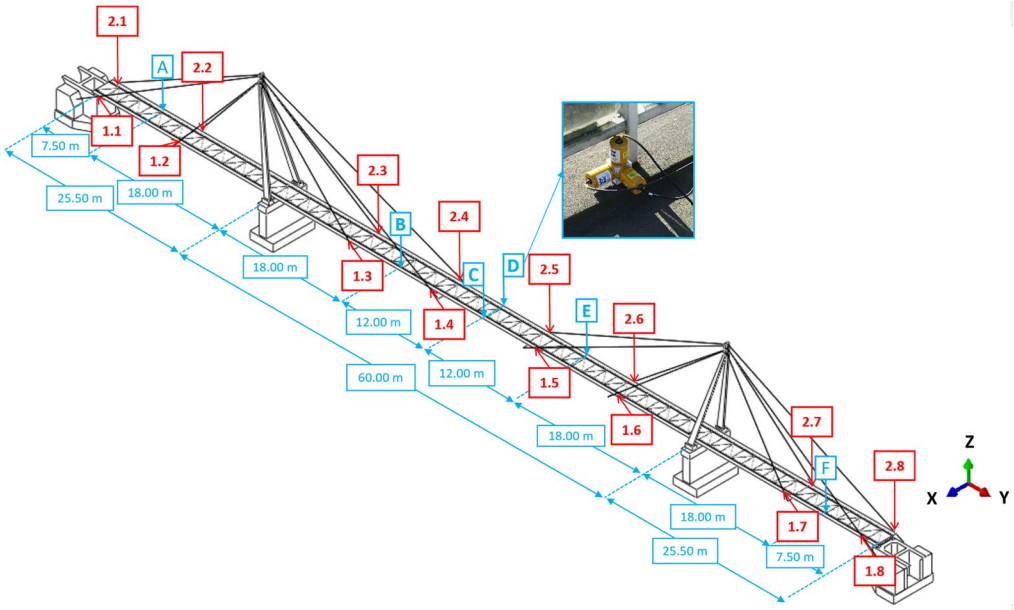

(a)

(b)

Fig. 5 In-field experimental tests of the footbridge: (**a**) configurations of measurement points; (**b**) RSV-150 laser Doppler vibrometer

complex vectors (see Eq. 11). This application is valuable for assessing the similarity between mode shape vectors for two modal models A and B ($\{\psi_i^A\}, \{\psi_i^B\}$) that are arbitrarily scaled, as high MAC_{ij} values indicate similarity between mode shapes [57]. Since, the MAC_{ij} (Eq. 12a) metric can be calculated for the modes whose similarity is under consideration, hence, the MAC matrix (Eq. 12b) is an evaluator determining the modal models' global similarity. The MAC indicator is used for modal correlation in two main cases: (1) to assess the impact of loading and environmental conditions on experimental modal models, and (2) to enhance and revise numerical modal models to minimize discrepancies with the real object. Ideally, MAC values for corresponding vibration modes should be close to 100% along the main diagonal and near 0% outside it. The $Auto - MAC$ matrix validates the modal model, with off-diagonal elements ideally approaching 0%:

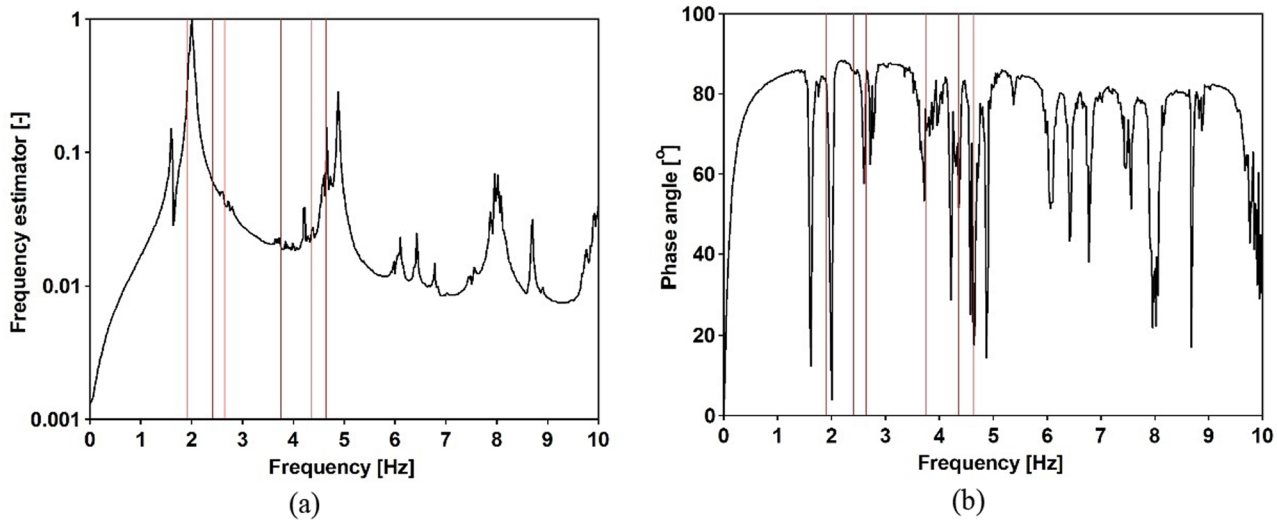

Fig. 6 Modal parameters estimation: (**a**) normalized summation for all combinations of auto- and cross-spectral density functions; (**b**) phase angle

$$MAC_{ij}(\psi_i^A, \psi_j^B) = \frac{\left(\left\{\psi_i^A\right\}^T \left\{\psi_j^B\right\}\right)^2}{\left(\left\{\psi_i^A\right\}^T \left\{\psi_i^A\right\}\right)\left(\left\{\psi_j^B\right\}^T \left\{\psi_j^B\right\}\right)} \tag{12a}$$

$$MAC(\psi_i^A, \psi_j^B) = \begin{pmatrix} MAC_{11} & \cdots & MAC_{1j} \\ \vdots & \ddots & \vdots \\ MAC_{i1} & \cdots & MAC_{ij} \end{pmatrix} \tag{12b}$$

Then, the phase scatter ratting for each mode was checked as 'low' based on the Modal Phase Collinearity (*MPC*) and the Mean Phase Deviation (*MPD*) functions (see Table 2). The *MPC* function serves to assess the complexity of modes. It quantifies the linear functional relationship between the real and imaginary components of the unscaled mode shape vectors. Ideally, the *MPC* value should be nearing 100% for real normal modes. Conversely, a low *MPC* index suggests a relatively complex mode, potentially attributable to local damping elements within the tested structure, errors in data measurement, or inaccuracies in the analysis procedure. The MPD function indicates how much the phase angles of each mode shape coefficient vary from their average value, providing insight into the phase scatter across the mode shape. For reliable normal modes, it is expected that this variance will be minimal, hovering close to 0°. The phase scatter is considered 'low' when the *MPC* exceeds 90% and the *MPD* is below 15°.

4.2 Force measurement in cables

Another in-field planned and conducted experiment aimed at determining the forces in the cables of the suspended footbridge [58]. During the tests, the free vibration responses for all cables were recorded. The cables were induced by an impulsive excitation—a strike on the stay. Based on the recorded responses, the natural frequencies of the stay cables were determined. The vibrations were registered based on contactless measurements with the RSV-150 laser Doppler vibrometer (LDV), (see Fig. 5b) and with the classical approach, using accelerometers attached to the cables (with the 356B18 triaxial accelerometer located one-quarter of the span of the stay cable). Subsequently, the forces in the cables were determined based on the vibration equation of a continuous rod stretched by force P (Eq. 13a) with zero boundary conditions (Eq. 13b, 13c):

$$EI\frac{d^4u}{dx^4} - P\frac{d^2u}{dx^2} - \rho\omega^2 u = 0 \tag{13a}$$

$$u(0) = u(l) = 0 \tag{13b}$$

$$u''(0) = u''(l) = 0 \tag{13c}$$

where:
ρ is the unit mass of the rod;
E is the Young modulus;
I is the cross-sectional moment of inertia;
l is the length of the rod;
u is the lateral displacement of the rod;
ω is the angular frequency of the rod.

The solution of Eq. 13 allows for estimation of the axial force for the $n-th$ experimental natural frequency of the rod, expressed by the following equation [59]:

$$P = P_{0n}\left(f_n^2 f_{0n}^{-2} - 1\right) \tag{14a}$$

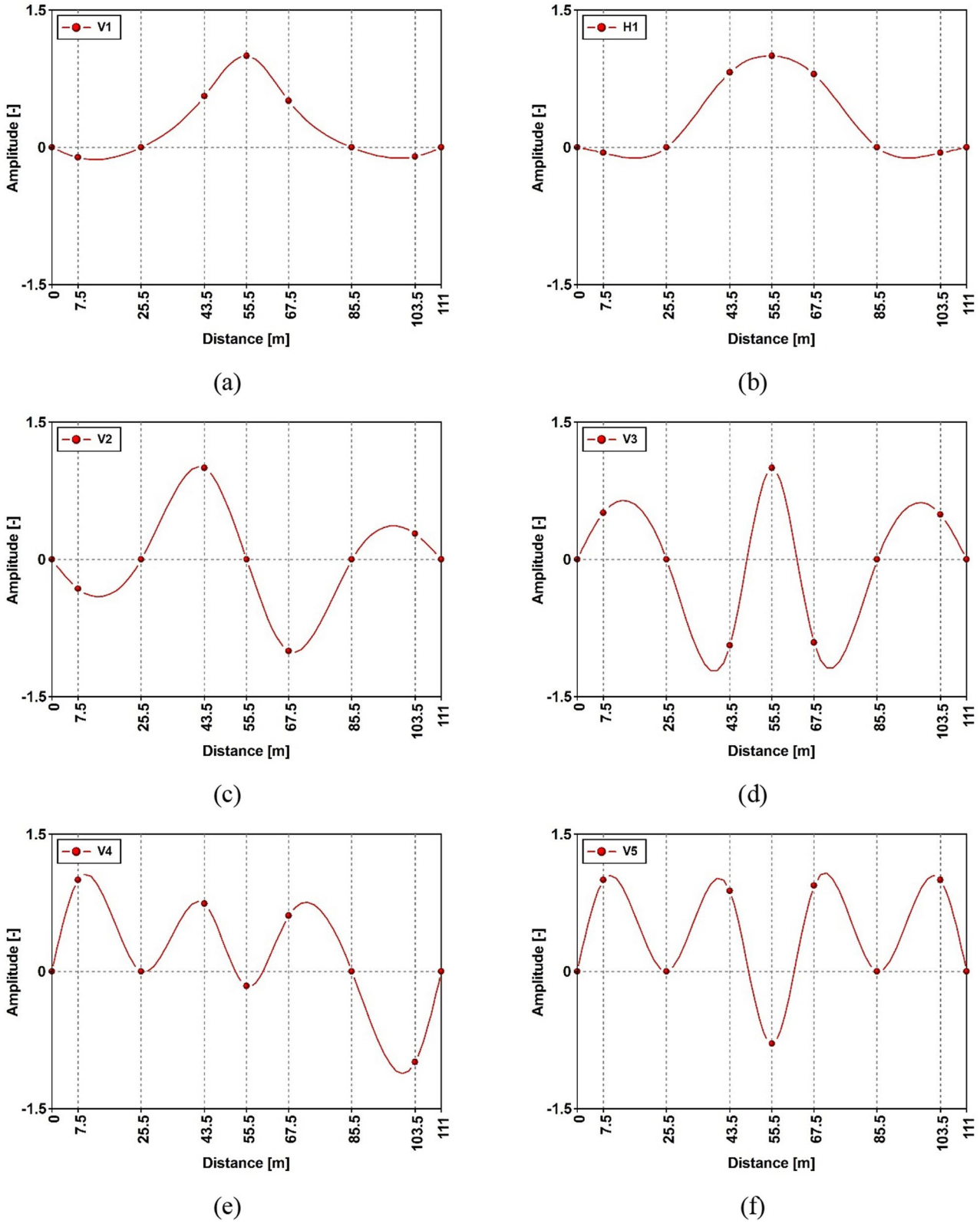

Fig. 7 Modes along A, B, C E and F alignment for: (**a**), (**c**), (**d**), (**e**), (**f**) vertical and (**b**) horizontal direction

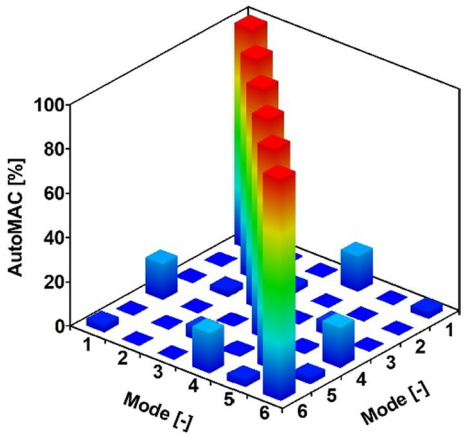

Fig. 8 *Auto* − *MAC* matrix (3D representation)

$$P_{0n} = EIn^2\pi^2 l^2 \tag{14b}$$

$$f_{0n}^2 = (n\pi l^{-1})^4 EI\rho^{-1}/2\pi \tag{14c}$$

where:

f_n is the $n-th$ experimental natural frequency of the rod.

In Fig. 9, the modal model estimators, i.e., normalized auto-spectral density functions obtained due to contactless and contact measurements are presented for the first set of cables, i.e., 1.1, 1.2, 1.3 and 1.4 (see Fig. 5a). Based on the findings, it can be concluded that both methods, contactless measurements with the RSV-150 laser Doppler vibrometer (LDV) and the classical approach using accelerometers attached to the cables, yielded consistent results (see Fig. 9). This suggests that both methods are equally effective for measuring vibrations in the given scenario. Such congruence in results enhances confidence in the accuracy and reliability of the measurement techniques employed. In Table 3, the values of forces in all cables obtained from the tests are compared with those from design documentation. Since two modes were used for estimating the tension in the cables, the final force value was calculated as the mean of the two evaluations. In general, good agreement can be observed between the measured values and the stay cable tensions according to the design values. However, the procedure was applied to all cables. Hence, despite the structure being symmetrical, some differences in force values were found (see Table 3). This can be explained by some inaccuracies that occurred during the realization of the cable tensions, as well as some changes that can occur during the structures' usage.

4.3 Dynamic susceptibility of the footbridge to pedestrian walking

The final stage of in-field tests was the assessment of the footbridge responses to pedestrian traffic. Based on previously elaborated model of the structure (see Table 2), the load cases were chosen for the investigation. The comparative analysis utilized acceleration time histories obtained from specific control points on the footbridge deck (refer to Fig. 5a). Through various literature sources and standard technical design procedures, the parametric numerical results were hence assessed in terms of conventional performance indicators relevant to vibration serviceability considerations.

Within the scope of present study, which included pedestrian passages, the acceleration time histories, i.e., $a(t)$, were initially examined to determine the Peak Value Acceleration (PAV, Eq. 15a). Subsequent comparisons were made among the selected loading approaches, with a focus on the root mean squared (RMS) acceleration values (Eq. 15b). In addition, the $CREST$ factor (Eq. 15c) was applied for an assessment of the waveform of $a(t)$ obtained from different loading cases induced by walking users:

$$\mathrm{PAV} = \max\left(|\mathrm{a(t)}|\right) \tag{15a}$$

$$\mathrm{RMS} = \left[\frac{1}{\Delta \mathrm{t}} \int_{\mathrm{t_1}}^{\mathrm{t_1}+\Delta \mathrm{t}} [\mathrm{a(t)}]^2 \mathrm{dt}\right]^{\frac{1}{2}} \tag{15b}$$

$$\mathrm{CREST} = \frac{\mathrm{PAV}}{\mathrm{RMS}} \tag{15c}$$

In Table 4, results are presented in terms of dynamic performance indicators (defined by Eq. 15a.b.c) for the

Table 2 Dynamic characteristics of the footbridge

Mode $i[-]$	Type $[-]$	Frequency $f_i^{OMA}[Hz]$	Damping ratio $\varsigma[\%]$	MPD $[\circ]$	MPC $[\%]$	Scatter
1	V1	1.91	1.46	0.91	99.97	low
2	H1	2.35	1.26	8.39	98.55	low
3	V2	2.57	1.23	2.36	99.84	low
4	V3	3.80	1.19	2.80	99.77	low
5	V4	4.35	0.53	3.57	99.67	low
6	V5	4.65	0.43	1.57	99.92	low

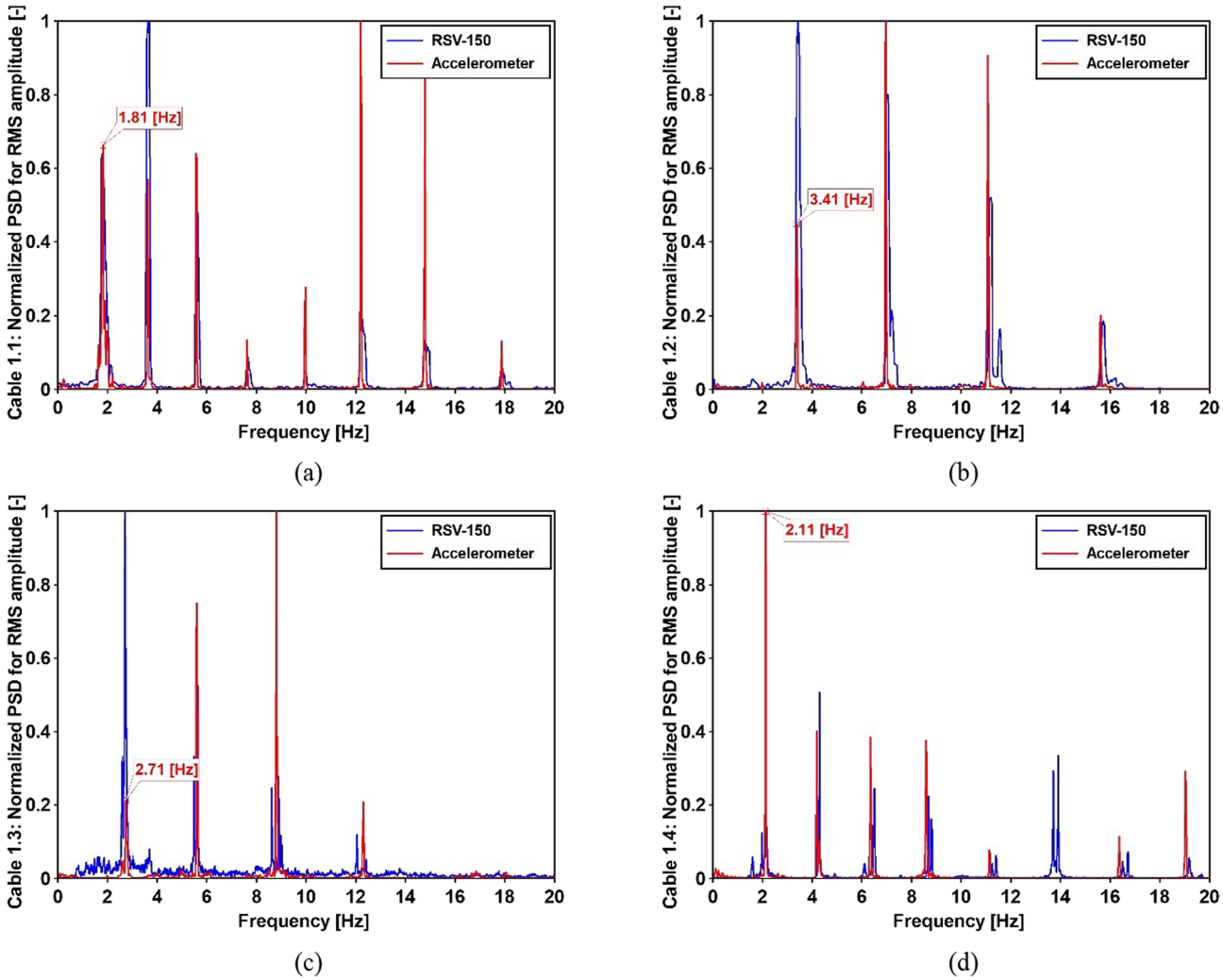

Fig. 9 Normalized auto-spectral density functions for cable: (**a**) 1.1; (**b**) 1.2; (**c**) 1.3 and (**d**) 1.4

Table 3 Values of forces in the cables

Cable	Force [kN]		Cable	Force [kN]	
	In-field test	Design		In-field test	Design
1.1	233.42	230.17	2.1	243.59	230.17
1.2	232.61	220.69	2.2	241.10	220.69
1.3	214.16	210.01	2.3	215.76	210.01
1.4	326.07	360.04	2.4	358.01	360.04
1.5	354.75	360.04	2.5	367.89	360.04
1.6	206.27	210.01	2.6	217.36	210.01
1.7	217.44	220.69	2.7	231.21	220.69
1.8	218.57	230.17	2.8	264.57	230.17

vertical direction at the control points B and C (Fig. 5a). In Fig. 10, the obtained results for the investigated variants are also presented in the frequency domain. In Fig. 11, the analysis for two pedestrians under the resonant frequency loading case is finally presented. Based on this approach one can determine the frequency characteristics of the forces generated by a walking user, in terms of resonance phenomena.

Once the signals were recorded, the quality of the collected data was analyzed in the time and frequency domains. First, to eliminate unwanted noise, the signals were filtered using a second-order low-pass filter with a cutoff frequency of 10 Hz. Next, the frequency domain characteristics were verified (see Fig. 10a, b). Based on this analysis, the critical frequency that could affect the structure was identified. For this case, a second round of signal filtering was performed. The cutoff frequency of 5 Hz was used, since the second-order effect of human-induced loading was not neglected either. From these final products, the PAVs, RMSs, and CREST factors were extracted (see Table 4). Furthermore, the data were

Table 4 Experimental assessment of the footbridge responses to pedestrian traffic

Variant	Number of pedestrians and type of motion	$f[Hz]$	PAV [m/s^2]		RMS [m/s^2]		CREST [–]	
			B	C	B	C	B	C
1	walking of 1 pedestrian with a random frequency	–	0.08	0.09	0.04	0.05	2.00	1.80
2	walking of 4 pedestrians with a random frequency	–	0.12	0.14	0.07	0.09	1.71	1.56
3	walking of 1 pedestrian with the resonant frequency	1.91	0.22	0.29	0.11	0.18	2.00	1.61
4	walking of 2 pedestrians with the resonant frequency	1.91	0.34	0.56	0.18	0.32	1.89	1.75

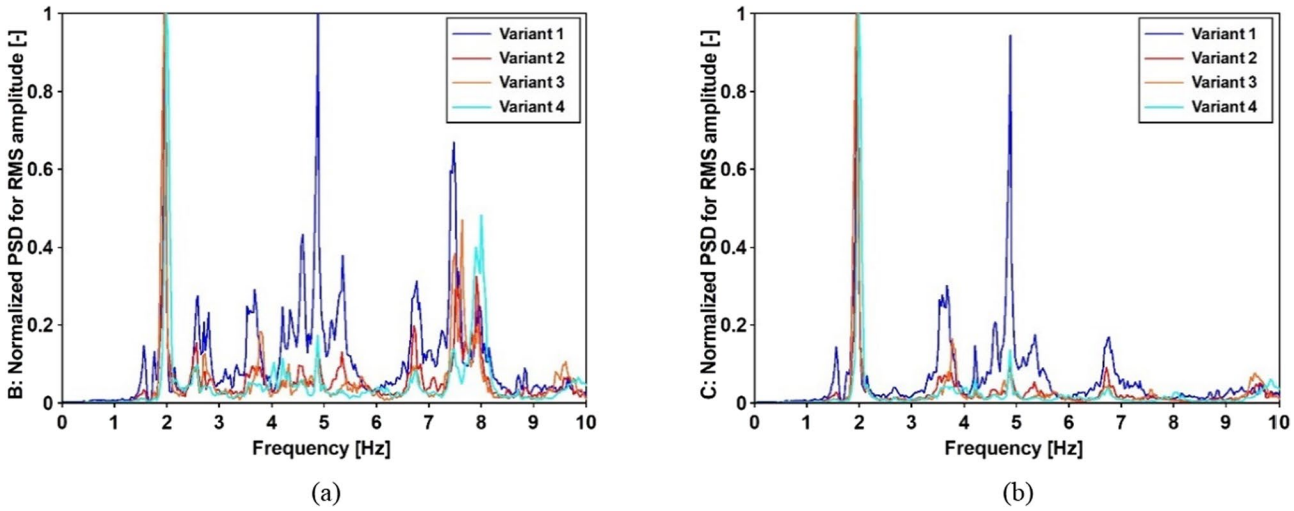

Fig. 10 Normalized auto-spectral density functions for control points: (**a**) B and (**b**) C

analyzed using the short-time Fourier transform (STFT) to observe how the frequency content of a nonstationary signal varies over time (see Fig. 11). For variants no. 3 and 4, when the resonant performance was initiated, the pedestrians' passages were controlled. All passages were synchronized with a metronome to achieve a frequency step of 1.91 Hz.

Based on the results from the in-field assessment of the footbridge, including OMA tests (see Table 2) and experimental tests measuring its response to pedestrian traffic (see Table 4 and Fig. 10), it was confirmed that the footbridge is primarily susceptible to vertical forces generated by pedestrians. This observation is further supported by SETRA's recommendation [38], where the structure's first horizontal mode (2.35 Hz) is classified as 'low risk of resonance under standard loading conditions'.

5 Parametric numerical investigation

5.1 FE modeling, experiment–theory comparison, and model tuning

A three-dimensional FE model, incorporating essential components of the footbridge, was assembled using the ABAQUS/Standard software program [60]. The FE model was formulated using the following presumptions: the four-nodes shell finite elements were applied to model the concrete slab, the steel girders, the cross-bars, and the steel pylons; the truss elements with non-compression material options were used to model the cables; the boundary conditions between the pylons and the abutments, and the footbridge piers were assumed as fixed; the boundary conditions between the four external footbridge cables and the abutments, as well as the connections between the twelve interior cables and the cross bars were assumed as pinned; the tie interaction option was used between the concrete deck and the main girders. The material parameters were adopted in accordance with the design documentation. The conventional Rayleigh model of damping

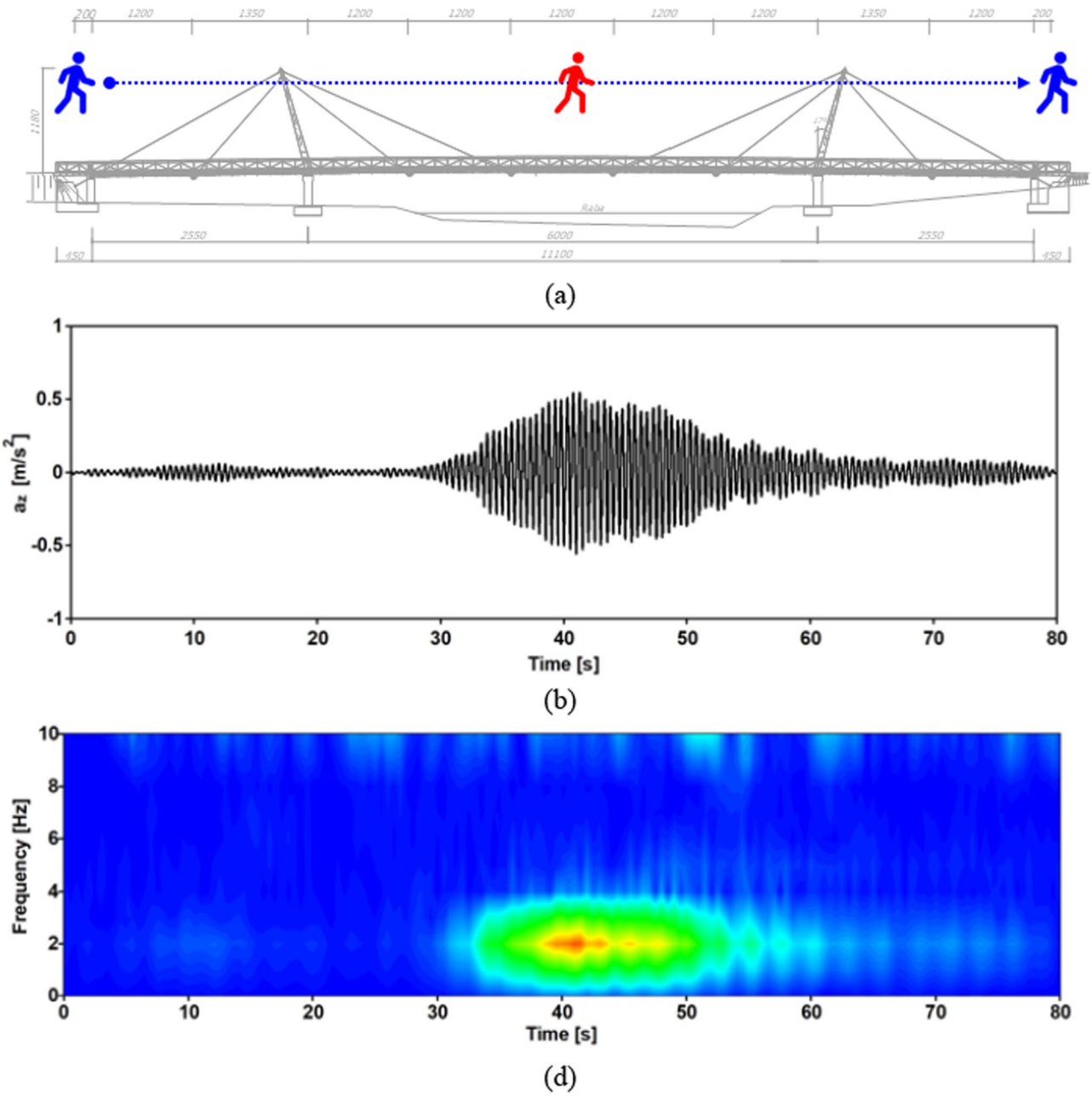

Fig. 11 Walking of 2 pedestrians with the resonant frequency: (**a**) side view for the passage; (**b**) time history of accelerations registered in point C; (**c**) short-time Fourier transform (STFT) for the data registered in point C

with coefficients α (for mass-proportional damping) and β (for stiffness-proportional damping) was applied as material characteristic for the numerical simulation purposes. Damping ratio values were adopted from the experimental modal model. The following values of coefficients were applied: $\alpha = 0.29673$, $\beta = 0.0004$ for the 1st and 3rd natural frequency of the footbridge (see Table 2). These values were extracted from [60]

$$\begin{cases} \alpha = 4\pi f_1 f_3 \frac{\varsigma_1 f_3 - \varsigma_3 f_1}{f_3^2 - f_1^2} \\ \beta = \frac{\varsigma_3 f_3 - \varsigma_1 f_1}{\pi (f_3^2 - f_1^2)} \end{cases} \tag{16}$$

The results from the experiment–theory comparison in terms of efficiency in FE modeling analysis are presented in Fig. 12 and summarized in Table 5. The similarity of experimental vs. numerical modal models of the structure was checked for two variants of FE modelling approach,

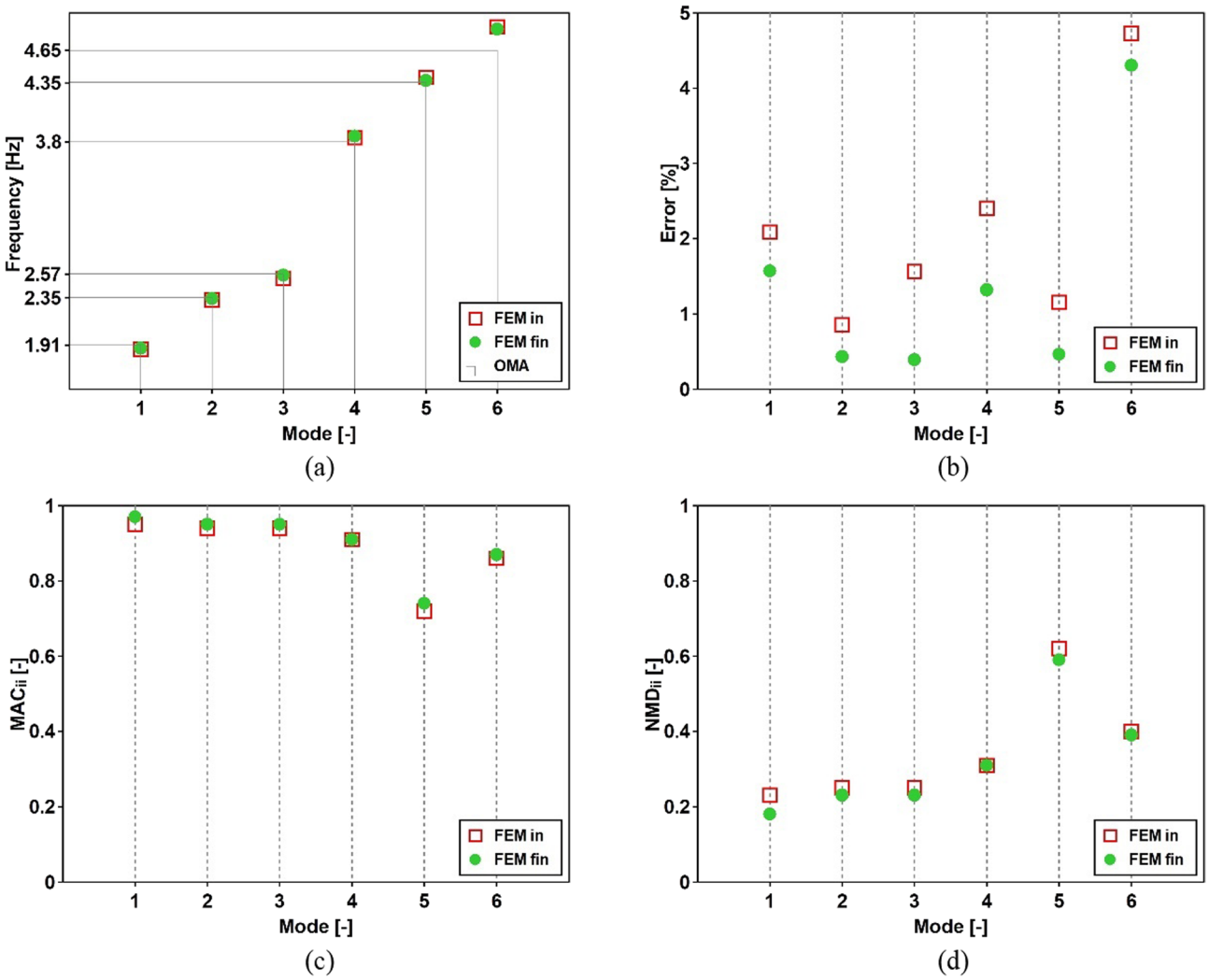

Fig. 12 Comparison of experimental and theoretical dynamic characteristics (initial vs. final FE model). (**a**) Natural frequencies; (**b**) error; (**c**) MAC (see Eq. 12a) values and (**d**) NMD (see Eq. 17) values

Table 5 Comparison of experimental and theoretical dynamic characteristics

Mode $i[-]$	Frequency $[Hz]$			Error $[\%]$		$MAC_{ii}[-]$		$NMD_{ii}[-]$	
	f_i^{OMA}	$f_i^{FE_{in}}$	$f_i^{FE_{fin}}$	FE_{in}	FE_{fin}	FE_{in}	FE_{fin}	FE_{in}	FE_{fin}
1	1.91	1.87	1.88	2.09	1.57	0.95	0.97	0.23	0.18
2	2.35	2.33	2.34	0.85	0.43	0.94	0.95	0.25	0.23
3	2.57	2.53	2.56	1.56	0.39	0.94	0.95	0.25	0.23
4	3.80	3.84	3.85	2.40	1.32	0.91	0.91	0.31	0.31
5	4.35	4.40	4.37	1.15	0.46	0.72	0.74	0.62	0.59
6	4.65	4.87	4.85	4.73	4.30	0.86	0.87	0.40	0.39

i.e., without accounting for the forces in cables (FE_{in}) and with the forces introduced (FE_{fin}). The tension forces in the cables were introduced using the predefined field procedure implemented in the ABAQUS/Standard software program. The evaluation and tuning of the FE model were investigated based on comparison of natural frequencies and mode sets. To compare the outcome modes of FE model (see Fig. 13) and OMA (see Fig. 7), besides using the MAC, the Normalized Modal Difference (NMD) was also applied. The NMD is related to the MAC by the following relation:

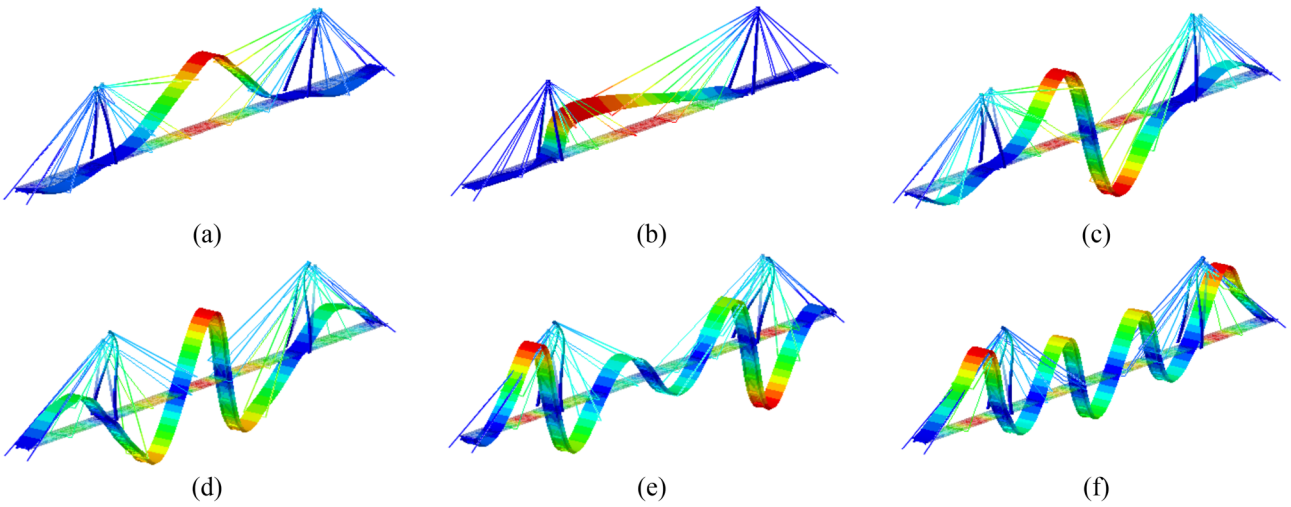

Fig. 13 Mode shapes of a FE_{fin} model for the frequency: (**a**) $f_1 = 1.88[Hz], m_{1\alpha} = 24.85[10^3 kg]$; (**b**) $f_2 = 2.34[Hz], m_{2\alpha} = 36.47[10^3 kg]$; (**c**) $f_3 = 2.56[Hz], m_{3\alpha} = 31.94[10^3 kg]$; (**d**) $f_4 = 3.85[Hz], m_{4\alpha} = 35.69[10^3 kg]$; (**e**) $f_5 = 4.37[Hz], m_{5\alpha} = 32.56[10^3 kg]$ and (**f**) $f_6 = 4.85[Hz], m_{6\alpha} = 41.58[10^3 kg]$

Table 6 Bachman model parameters for walking according to [20]

$G[kN]$	α_1	α_2	α_3	φ_1	φ_2	φ_3
0.83	0.37	0.10	0.12	0	$\pi/2$	$\pi/2$

Table 7 SMD parameters for the step frequency $f = 1.88Hz$ and $M = 85kg$

Parameter	Model				
	SMD-0	SMD-1	SMD-2	SMD-3	SMD-4
$m[kg]$	85	59	39	70	85
$c[Ns/m]$	1478	1068	574	746	977
$k[N/m]$	11,088	17,622	10,762	23,965	12,600

$$NMD\left(\psi_i^A, \psi_j^B\right) = \sqrt{\frac{1 - MAC_{ij}(\psi_i^A, \psi_j^B)}{MAC_{ij}(\psi_i^A, \psi_j^B)}} \tag{17}$$

Better compatibility to the experimental modal model was confirmed for the second approach. Hence, the incorporation of tension forces in footbridge cables has enhanced the quality of FE model that was finally used for the research purposes. The numerical modal model with modal masses for each mode and natural frequency is shown in Fig. 13.

Table 8 SMD parameters for the step frequency $f = 2.00Hz$ and M = 85 kg

Parameter	Model				
	SMD-0	SMD-1	SMD-2	SMD-3	SMD-4
$m[kg]$	85	55	31	69	85
$c[Ns/m]$	1125	1006	164	737	951
$k[N/m]$	12,064	16,924	12,116	23,559	13,100

5.2 Application of SMD pedestrian load model for vibration assessment of the footbridge

Based on both experimental and numerical modal models of the footbridge, the primary characteristics of user motion, such as walking frequency, were fitted for further investigation. The results from in-field tests dedicated to assessing the dynamic susceptibility of the footbridge to pedestrian walking were also taken into account. Therefore, two types of walking passages were simulated numerically, i.e., (1) 1.88 [Hz]—to induce dynamic resonant response and (2) 2.0 [Hz]—to induce dynamic responses outside the resonance range. The mass of the pedestrian is assumed as $M = 85$ $[kg]$ In the traditional force model (FM) the pedestrian is simulated by a concentrated force with the amplitude calculated based on Eq. 2 with parameters according to Bachman proposal [20] assembled in Table 6. The parameters of the analysed SMD-0:4 models [lumped mass (m) spring stiffness (k) and damping term (c)], determined according to formulas 4–10 for assumed mass and step frequencies are collated in Tables 7 and 8, respectively. The numerical analyses for all investigated configurations were conducted using ABAQUS/Standard. To account for the mass–structure interaction and inertia

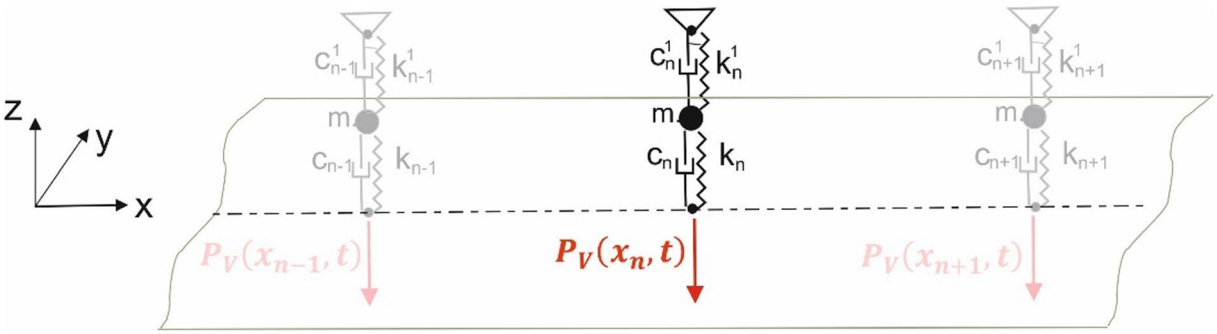

Fig. 14 SMD realization in the FEM model with the user elements

Table 9 SMD parameters for the step frequency $f = 1.88Hz$ and M = 74 kg

Parameter	Model				
	SMD-0	SMD-1	SMD-2	SMD-3	SMD-4
$m[kg]$	74	56	31	60	74
$c[Ns/m]$	1478	1015	500	644	858
$k[N/m]$	11,088	17,028	8254	20,336	11,000

effect of a moving mass in SMDs the user element U_{el} was coded for the implicite dynamic procedure and introduced into FEM analysis. The stiffness (k) and damping (c) matrices of the user two-node element are defined as a function of time, which allows for element activation and deactivation at predefined time instances.

For the numerical simulations of actions representing the passage of one pedestrian it was assumed that a vertical force $P_v\ (x,\ t)$ is moving across the span of the structure at a constant speed (see Eq. 1). For all applied models the step length is assumed as 0.75 [m], for both analysed step frequencies. For the SMD models, 145 point masses m are placed over prospective step points along the deck. Every lumped mass constitutes a node of two user elements (see Fig. 14). The first one (with parameters k_n and c_n) connects the mass to the deck step point, activates at the beginning of the appropriate time step instance and remains active throughout the step time length (see Eq. 18b, c). The second one connects the mass to a fixed point over it, and is active at all times except the span of this time step. This second element (with large stiffness k_n^1 and damping c_n^1) is included for computational reasons. The vertical nodal force generated in the user element linking the mass with the deck during the $n-th$ time ste, starting at the time instant t_n takes the form:

$$F_n = k\left(\Delta z(t) - \Delta z(t_n)\right) + c\left(\Delta v_z(t) - \Delta v_z\left(t_n\right)\right) \tag{18a}$$

$$k_n = \begin{cases} k\ for\ \ t_n \le t \le t_{n+1} \\ 0\ \ for\ t\ < t_n\ or\ t > t_{n+1} \end{cases} \tag{18b}$$

$$c_n = \begin{cases} c\ \ for\ t_n \le t \le t_{n+1} \\ 0\ \ for\ t < t_n\ or\ t > t_{n+1} \end{cases} \tag{18c}$$

where m, k, c are the SDM parameters (according to Tables 7 and 8), $\Delta z(t)$, Δv_z are relative vertical displacement and velocity of the element nodes, and $\Delta z(t_n)$, $\Delta v_z(t_n)$ are the element elongation and relative velocity at the beginning of the step, added to ensure that at this moment the pedestrian (lumped mass) has the position and velocity complying with these of the deck step point (Table 9).

5.2.1 Dynamic actions representing resonant performance

Resonant conditions are the most appropriate states for assessing the dynamic performance of footbridges in terms of comfort criteria [41]. Therefore, the periodic human-induced loading with a frequency equal to the mode identified as most critical was examined. Based on both experimental (see Table 2 and Fig. 7) and numerical (see Table 5 and Fig. 13) modal models of the footbridge, the primary characteristics of user motion, such as frequency, were fitted for further investigations. The results from in-field tests dedicated to assessing the dynamic susceptibility of the footbridge to pedestrian walking were also taken into account (see Fig. 10). For parametric numerical simulations of resonant states, the natural frequency equal to 1.88 [Hz], corresponding to the first vertical mode shape, was utilized.

Three types of user motions on the footbridge were simulated numerically, namely: (1) the passage of a single pedestrian; and (2) the passage of two perfectly synchronized pedestrians, (3) a single user-induced pulsating force, applied at the center of the mid-span section of the footbridge, so as to induce steady-state resonant conditions. The choice of the third load model is based on the fact that the

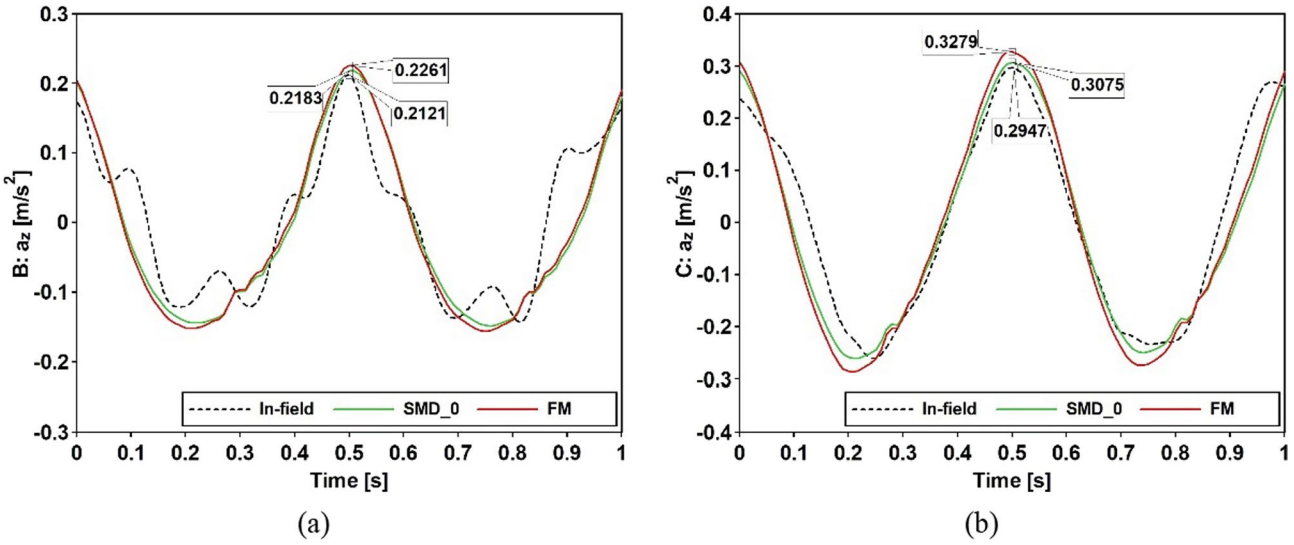

Fig. 15 Segment of the time history (TH) cantered around (±0.5 [s]) the PAV for control points B (**a**) and C (**b**) that was recorded during the passage of a single pedestrian with a resonant frequency

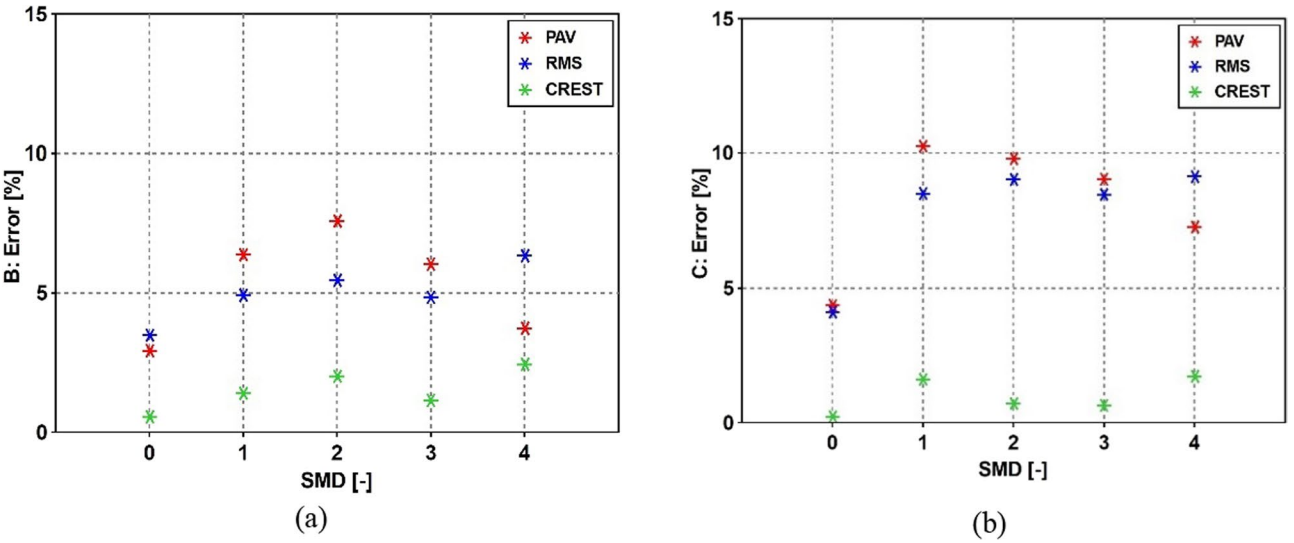

Fig. 16 Passage of a single pedestrian with a resonant frequency: comparison of the SMD models and in-field testing, based on PAV, RMS, and CREST indicators, for control points B (**a**) and C (**b**)

analysis of the footbridge's dynamic response under steady-state resonant conditions is recommended by official technical standards SÉTRA 2006 [41] and BS NA EN 1991–2 [43], particularly concerning the dynamic loads induced by crowds.

First, the passage of a single pedestrian, with a resonant frequency, was investigated. In Fig. 15, the time histories (TH) of acceleration centered around (±0.5 [s]) the peak acceleration value (PAV) for control points B and C are provided for in-field measurement as well as SMD-0 and force (FM) models. This critical segment of the acceleration time history was selected for comparative analysis between the SMD models and in-field testing (see Fig. 16) and the Force Model (FM) results (see Fig. 17). It was observed that the SMD-0 exhibited the strongest correlation with the in-field results for all investigated indicators, including peak acceleration values (PAV), root mean square (RMS), and CREST factor, in both analyzed points B (Fig. 16a) and C (Fig. 16b). For this comparison, the differences did not exceed 5 [%]. When considering the similarity of SMD models to the commonly used Force Model (FM), it was observed that, results obtained with SMD-0 differ most form FM results

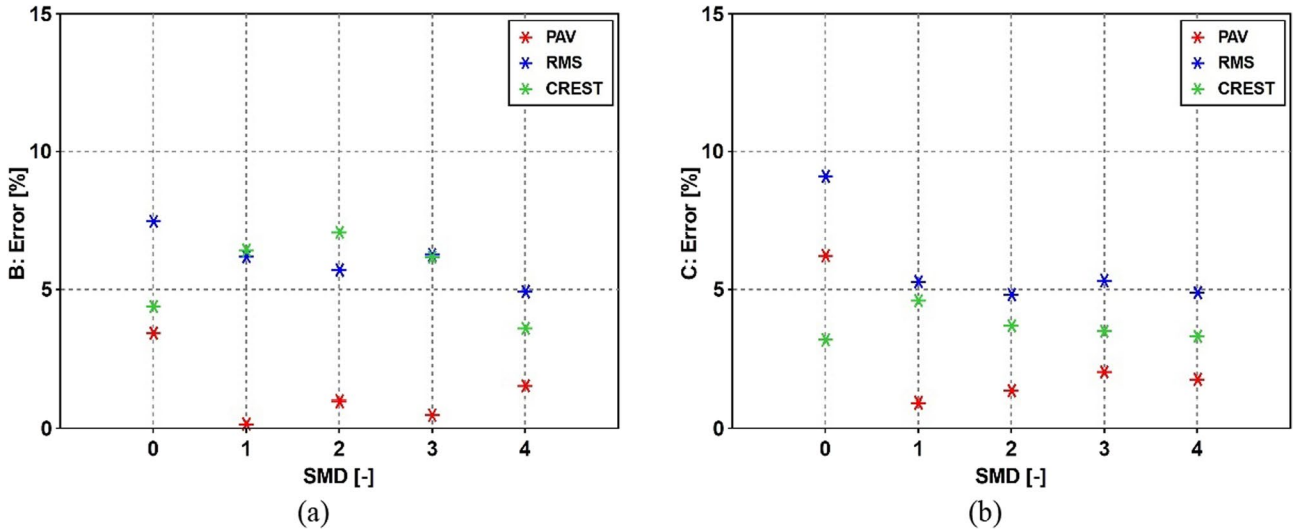

Fig. 17 Passage of a single pedestrian with a resonant frequency: comparison of the SMD models and the Force Model (FM), based on PAV, RMS, and CREST indicators, for control points B (**a**) and C (**b**)

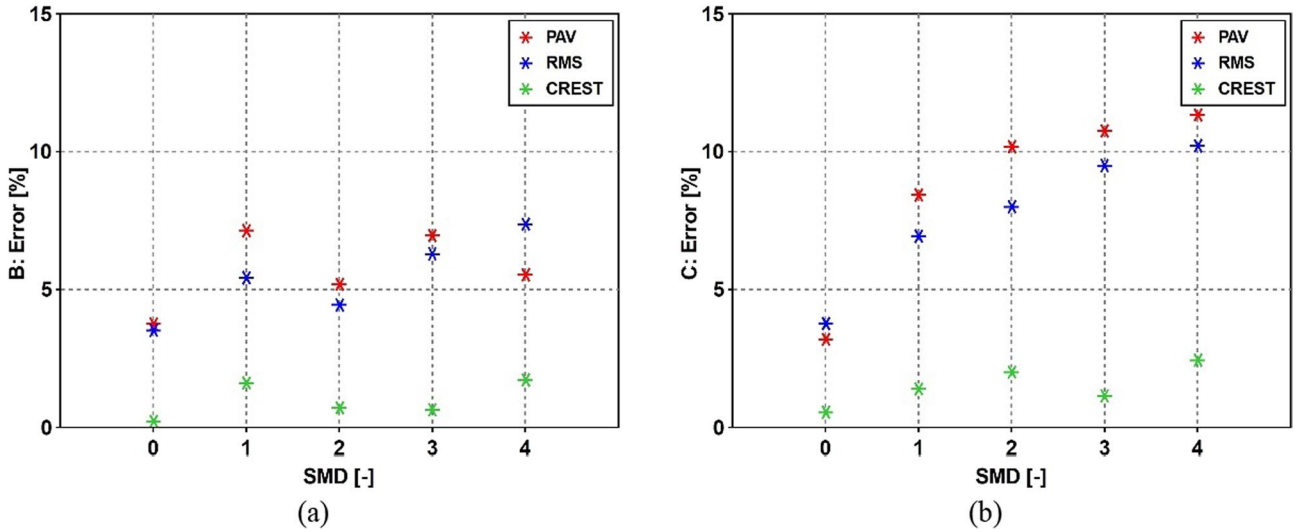

Fig. 18 Passage of two perfectly synchronized pedestrians with a resonant frequency: comparison of the SMD models and in-field testing, based on PAV, RMS, and CREST indicators, for control points B (**a**) and C (**b**)

in terms of PAV and RMS indicators in both control points (see Fig. 17).

The results for the second loading scenario, passage of two synchronized pedestrians walking with a resonant frequency, are presented in Fig. 18 also in terms of comparative analysis referred to the in-field testing. In addition, in this case the SMD-0 model shows the strongest consistency the in-field results for all investigated indicators (PAV, RMS, and CREST factor) in both analyzed points: B (Fig. 18a) and C (Fig. 18b). with the differences below 5 [%].

In the analysis of the dynamic response to a pulsating load applied to the center of the footbridge it is important to note that this assessment is conducted by applying a pulsating distributed load to the deck of the footbridges for a sufficient duration to achieve steady-state conditions. Consequently, depending on the size of the footbridge, other factors such as additional mass or damping effects can influence the dynamic response of the footbridge. However, in this study, the effectiveness of SMD models compared to the Force Model (FM) in terms of steady-state resonance for assessment indicators (PAV, RMS, CREST) and the time of diagram stabilization

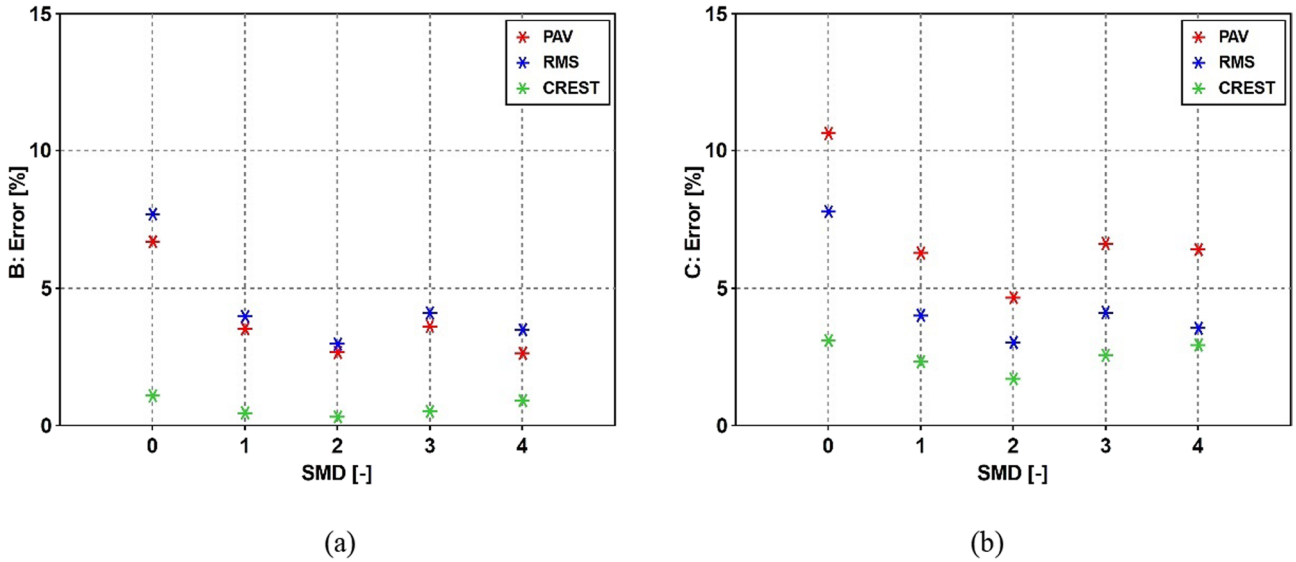

Fig. 19 Steady-state modelling with resonant frequency: comparison of the SMD models and the force model (FM), based on PAV, RMS, and CREST indicators, for control points B (**a**) and C (**b**)

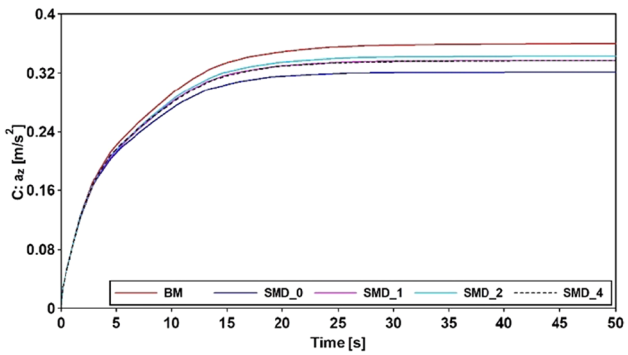

Fig. 20 Performance of the steady-state resonance stabilization time based on the envelopes of time history acceleration

was evaluated (see Figs. 19 and 20). For both B and C control points, it was observed that the largest difference between solutions extracted based on the FM and SMD models occurred for SMD-0 (see Fig. 19). The differences were estimated at point C (Fig. 19b) as 10.64 [%] for PAV, 7.77 [%] for RMS, and 3.11 [%] for the CREST factor. Regarding the time of steady-state resonant stabilization, it was observed that all analyzed models exhibit similar performance (see Fig. 20).

5.2.2 Dynamic actions representing typical human walking frequency

As provided by current literature [5], the most typical walking frequency for human normal walking is equal to 2 [Hz]. Despite this frequency not being resonant, numerical investigation with the SMD models was prepared for this case as well. The critical segments of the numerically extracted time history of acceleration were chosen for the comparative analysis of the SMD models, referencing Force Model (FM) results. In Fig. 21, the performances of SMD models for simulations of single pedestrian passage with a frequency of 2 [Hz] are collected for points B and C, respectively. The results from steady-state modelling are presented in Fig. 22. For both tasks the differences between all SMD and FM models are insignificant; below 3% for the pedestrian passage task and below 4% for the steady-state pulsating case.

6 Conclusions

This paper explored the application and accuracy of SMD pedestrian load models for assessing human-induced vibrations in cable-stayed footbridges. The comparative analysis of five selected SMD models was carried out to assess their influence on the calculated dynamic response of the structure. The assessment of these models performed (towards a recent "SMD-0" literature model, calibrated on the base of uncoupled body-motion records only) based on the analysis of percentage scatter in various indicators that are commonly used for comfort criteria performance, i.e., PAV, RMS, and CREST factor. Numerical simulations were conducted to assess both resonant and non-resonant influences on the structure. For each case, calculations were performed for pedestrian passages and steady-state loading conditions. The examination received strong support from in-field experimental tests concerning the tuning of the FE model and measurements of dynamic responses of the footbridge to pedestrian traffic. The obtained values were compared with experimental results

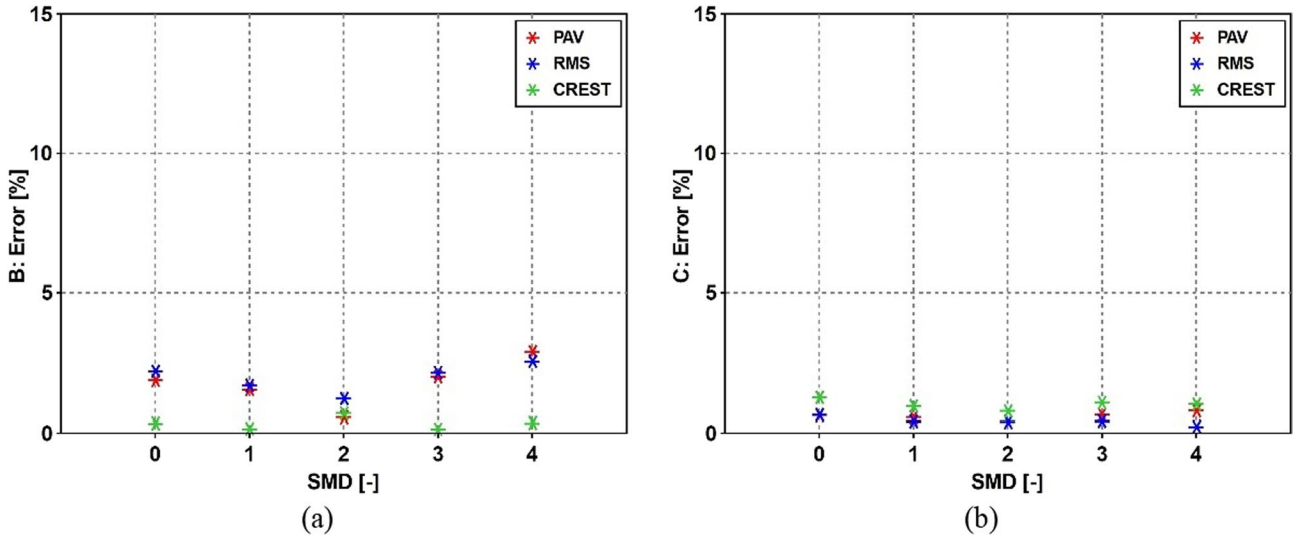

Fig. 21 Passage of a single pedestrian with 2 [Hz] pacing frequency: comparison of the SMD models and the force model (FM), based on PAV, RMS, and CREST indicators, for control points B (**a**) and C (**b**)

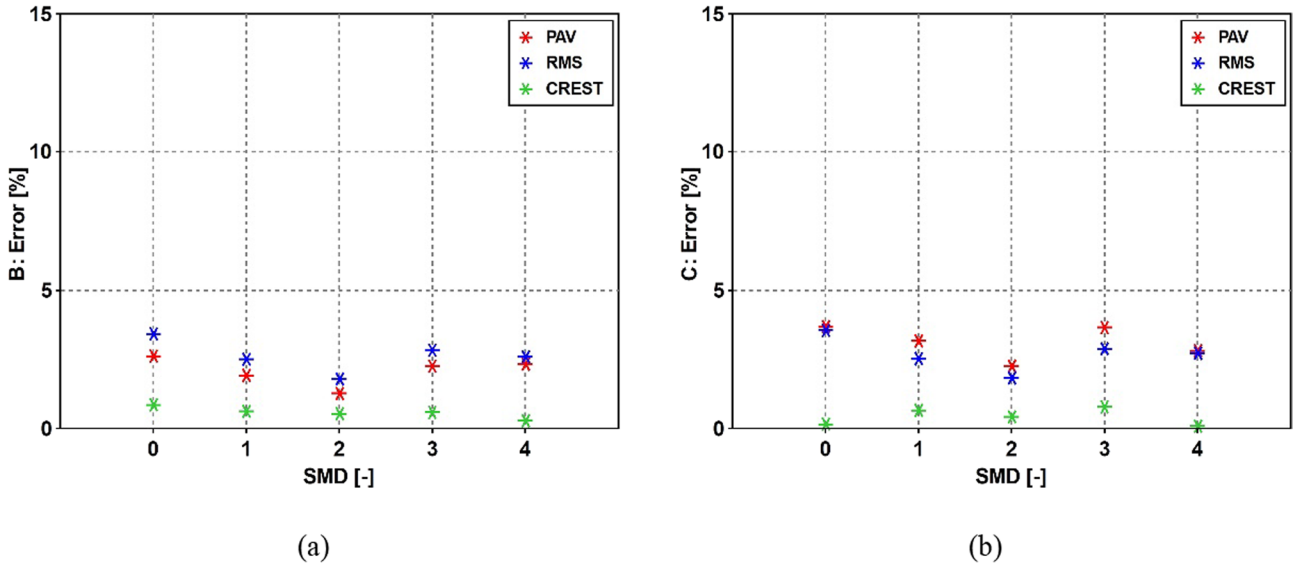

Fig. 22 Steady-state modelling with 2 [Hz] pulsating frequency: comparison of the SMD models and the force model (FM), based on PAV, RMS, and CREST indicators, for control points B (**a**) and C (**b**)

and with the dynamic response of the footbridge estimated based on Force Model (FM) simulations, which represent a conservative approach. From the study, the following remarks can be provided:

1. For the pedestrian passage, representing resonant performance, the study demonstrated that SMD models exhibit stronger correlations with experimental measurements (see Figs. 16, 18). Across all applied SMD models, the differences did not exceed 10% for all compared indicators. The most robust correlations were observed with the SMD-0 model, where differences did not exceed 5% in terms of in-field tests for both control points B and C.
2. In non-resonant frequency walking cases, the performance classification increased by one level and was lower than 5%. In many aspects, these results match with

the conclusions taken in the more advanced approaches for dynamic footbridge assessments from [26, 27] and [28].

3. The simulations of SMD load models for walking resonance frequencies benefited the assessment of vibration performance by significantly reducing the PAV and RMS values of the structure in numerical analyses. The highest average reductions in acceleration, when compared to a conservative FM solution, were on the order of 10% for the recently proposed [38] model SMD-0.
4. In conclusion, the SMD modelling approach stands out as a valuable strategy for accurately capturing human walking dynamics, potentially leading to more precise results and decreased conservatism in analysis, all while upholding safety standards. However, it is crucial to acknowledge that in this study, the method was primarily developed with a focus on individual pedestrian walking and does not account for parametrical changes in damping and mass characteristics of the footbridge resulting from user interactions, which are pivotal factors in assessing crowd conditions. Therefore, the subsequent phase will concentrate on addressing these aspects.

Most importantly, it was found that the SMD-0 model, which was applied to a real footbridge for the first time in this research contribution, achieved the best match with the in-situ results, while significant discrepancies were generally observed when considering a more conservative approach. At the same time, the employed SMD-0 model demonstrated to strongly reduce the typical parameterization of other SMD proposals, limiting the variation of input parameters to stiffness and damping, with the mass remaining constant. Such an optimizing feature is crucial for standardizing design procedures. This simplification can help to enhance the optimization of complex structural models under pedestrians while maintaining the necessary accuracy for practical engineering applications.

Acknowledgements The research study on SMD biodynamic model calibration is carried out in the framework of the Microgrant 2022 research project at University of Trieste, Department of Engineering and Architecture (Italy), "ComBioDyn: Experimental and numerical study for the calibration of biodynamic SDOF parameters and human–structure interaction phenomena on pedestrian systems of new generation" (PI Chiara Bedon). ComBioDyn research is carried out with the financial support of Friuli Venezia Giulia Region (Regione FVG-LR 2/2011, Art. 4, c. 2, lett. b)).

Funding University of Trieste and Friuli Venezia Giulia Region (Regione FVG-LR 2/2011, Art. 4, c. 2, lett. b), (PI Chiara Bedon).

Data availability Data will be shared upon request.

Declarations

Conflict of interest The authors declare that they have no conflict of interest.

Ethical approval This article does not contain any studies with human participants or animals performed by any of the authors.

Consent to participate and for publication All the authors agree to participate and publish.

References

1. Oviedo-Trespalacios O, Scott-Parker B. Footbridge usage in high-traffic flow highways: the intersection of safety and security in pedestrian decision-making. Transport Res F-Traf. 2017. https://doi.org/10.1016/j.trf.2017.06.010.
2. Bachmann H. 'Lively' footbridges – real challenge. Proc of Footbridge. 2002.
3. Caetano E, Cunha A. Dynamic Design of Slender Footbridges. Proc of ICSA. 2013.
4. Zhang B, Rasmussen B, Jorissen A, Harte A. Comparison of vibrational comfort assessment criteria for design of timber floors among the European countries. Eng Struct. 2013. https://doi.org/10.1016/j.engstruct.2013.03.028.
5. Feldmann M et al. Design of floor structures for human induced vibrations, JRC – ECCS joint report; 2009.
6. Wang L, He H, Li S. Structural vibration performance test based on smart phone and improved comfort evaluation method. Measurement. 2022. https://doi.org/10.1016/j.measurement.2022.111947.
7. Pańtak M. Elaboration of the vibration comfort criteria for footbridges during vibrations induced by pedestrians. Proc of IABMAS; 2012;2334–9.
8. Belykh I, Bocian M, Champneys AR, Daley K, Jeter R, Macdonald JHG, McRobbie A. Emergence of the London Millennium Bridge instability without synchronization. Nat Commun. 2021. https://doi.org/10.1038/s41467-021-27568-y.
9. Sánchez-Aparicio LJ, Ramos LF, Sena-Cruz L, Barros JO, Riveiro B. Experimental and numerical approaches for structural assessment in new footbridge designs (SFRSCC–GFPR hybrid structure). Compos Struct. 2015. https://doi.org/10.1016/j.compstruct.2015.07.041.
10. Bayat E, Milone A, Tubino F, Venuti F. Vibration serviceability assessment of a historic suspension footbridge. Buildings. 2022. https://doi.org/10.3390/buildings12060732.
11. Moutinho C, Cunha A, Caetano E, Carvalho JM. Vibration control of a slender footbridge using passive and semiactive tuned

mass dampers. Struct Control Health Monit. 2018. https://doi.org/10.1002/stc.2208.
12. Araújo MC Jr, Brito HMBF, Pimentel RL. Experimental evaluation of synchronization in footbridges due to crowd density. Struct Eng Int. 2009. https://doi.org/10.2749/101686609788957784.
13. Bocian M, et al. Time-dependent spectral analysis of interactions within groups of walking pedestrians and vertical structural motion using wavelets. Mech Syst Signal Process. 2018. https://doi.org/10.1016/j.ymssp.2017.12.020.
14. Pirner M, Fischer O. Wind-induced vibrations of concrete stress-ribbon footbridges. J Wind Eng Ind Aerodyn. 1998. https://doi.org/10.1016/S0167-6105(98)00079-8.
15. Uyttersprot J, De Corte W, Ingelbinck B. Influence of SLS design requirements on the material consumption and self-weight of web-core sandwich panel FRP composite footbridges. Compos Struct. 2021. https://doi.org/10.1016/j.compstruct.2020.113334.
16. Al-Rousan RZ, Al-Smadi YM, Laradhi AA. Operational modal analysis of the curved JUST footbridge induced by human. Procedia Manuf. 2020. https://doi.org/10.1016/j.promfg.2020.02.250.
17. Drygala IJ, Dulinska JM. A theoretical and experimental evaluation of the modal properties of a cable-stayed footbridge. Procedia Eng. 2017. https://doi.org/10.1016/j.proeng.2017.09.347.
18. Drygala IJ, Dulinska JM, Polak MA. Seismic assessment of footbridges under spatial variation of earthquake ground motion (SVEGM): experimental testing and finite element analyses. Sensors. 2020. https://doi.org/10.3390/s20041227.
19. Zivanovic S, Pavic A, Reynolds P. Vibration serviceability of footbridges under human-induced excitation: a literature review. J Sound Vib. 2005. https://doi.org/10.1016/j.jsv.2004.01.019.
20. Blanchard J, Davies BL, Smith JW. Design criteria and analysis for dynamic loading of footbridges, In: Proceedings of the DOE and DOT TRRL Symposium on Dynamic Behaviour of Bridges, Crowthorne, UK, May 19, 1977, pp. 90–106
21. Bachmann H, et al. Vibration problems in structures: practical guideline. Basel, Switzerland: Birkhäuser Verlag; 1995.
22. Bachmann H, Pretlove AJ, Rainer H. Dynamic forces from rhythmical human body motions. In Vibration Problems in Structures: Practical Guidelines; Birkhäuser: Basel, Switzerland, 1995; Appendix G.
23 Kerr SC, Bishop NWM. Human induced loading on flexible staircases. Eng Struct. 2001. https://doi.org/10.1016/S0141-0296(00)00020-1.
24 Pfeil PS, Varela WD, Costa NPA. Experimental calibration of a one degree of freedom biodynamic model to simulate human walking-structure interaction Eng. Struct. 2022. https://doi.org/10.1016/j.engstruct.2022.114330.
25. Shahabpoor E, Pavic A, Racic V. Interaction between walking humans and structures in vertical direction: a literature review. Shock Vib. 2016. https://doi.org/10.1155/2016/3430285.
26. Rezende FA, Brunet O Jr, Lopes Carvalho EM, Varela WD, Pereira AMB. Vibration-based sensitivity analysis of a flexible steel footbridge using probabilistic walking models. Eng Struct. 2024. https://doi.org/10.1016/j.engstruct.2023.117343.
27. Brunet O Jr, Rezende F, Carvalho EML, Varela WD, Pereira AMB. Probabilistic vibration performance assessment of a long-span steel footbridge. J Perform Constr Facil. 2022. https://doi.org/10.1061/(ASCE)CF.1943-5509.0001688.
28. Rezende F, Brunet O Jr, Varela WD, Pereira A, Carvalho E. Evaluation of TMD performance in footbridges using human walking probabilistic models. Vibration. 2021. https://doi.org/10.3390/vibration4020021.
29. Bedon C, Santos FA. Effect of spring-mass-damper pedestrian models on the performance of low-frequency or lightweight glazed floors. App Sci. 2023. https://doi.org/10.3390/app13064023.
30. Koopman B, Grootenboer HJ, de Jongh HJ. An inverse dynamics model for the analysis, reconstruction and prediction of bipedal walking. J Biomech. 1995. https://doi.org/10.1016/0021-9290(94)00185-7.
31. Brownjohn JMW, Chen J, Bocian M, Racic V, Shahabpoor E. Using inertial measurement units to identify medio-lateral ground reaction forces due to walking and swaying. J Sound Vib. 2018. https://doi.org/10.1016/j.jsv.2018.04.019.
32. Bocian M, Macdonald J, Burn J, Redmill D. Experimental identification of the behaviour of and lateral forces from freely-walking pedestrians on laterally oscillating structures in a virtual reality environment. Eng Struct. 2015. https://doi.org/10.1016/j.engstruct.2015.09.043.
33. Bocian M, Macdonald JHG, Burn JF. Biomechanically inspired modeling of pedestrian-induced vertical self-excited forces. J Bridge Eng. 2013. https://doi.org/10.1061/(ASCE)BE.1943-5592.0000490.
34. Geyer H, Seyfarth A, Blickhan R. Compliant leg behaviour explains basic dynamics of walking and running. Proc R Soc Biol Sci. 2006. https://doi.org/10.1098/rspb.2006.3637.
35. White RE, Alexander NA, Macdonald JHG, Bocian M. Characterisation of crowd lateral dynamic forcing from full-scale measurements on the Clifton Suspension Bridge. Structures. 2020. https://doi.org/10.1016/j.istruc.2019.11.012.
36. Wang L, Nagarajaiah S, Shi W, Zhou Y. Semi-active control of walking-induced vibrations in bridges using adaptive tuned mass damper considering human-structure-interaction. Eng Struct. 2021. https://doi.org/10.1016/j.engstruct.2021.112743.
37. Wang L, Zhou Y, Shi W. Random crowd-induced vibration in footbridge and adaptive control using semi-active TMD including crowd-structure interaction. Eng Struct. 2024. https://doi.org/10.1016/j.engstruct.2024.117839.
38. Bedon C. Single body sensor for calibration of Spring-Mass-Damper parameters in biodynamic pedestrian modelling. Measurement. 2023. https://doi.org/10.1016/j.measurement.2023.113258.
39. Galbraith FW, Barton MV. Ground loading from footsteps. JASA. 1970;48(5):1288–92.
40. ISO 10137:2007(E) - Bases for design of structures - Serviceability of buildings and walkways against vibrations
41. SÉTRA 2006: Assessment of Vibrational Behaviour of Footbridges under Pedestrian Loading. Technical Guide; Technical Department for Transport, Roads and Bridges Engineering and Road Safety: Paris, France, 2006
42. Eurocode 1: Actions on structures - Part 2: Traffic loads on bridges, (CEN, 2003)
43. BS NA EN 1991–2: UK National Annex to Eurocode 1. Actions on structures. Traffic loads on bridges. British Standards Institution.
44. Miyamori Y, Obata T, Hayashikawa T, Sato K. 2001. Study on identification of human walking model based on dynamic response characteristics of pedestrian bridges. In Proceedings of the Eighth East Asia-Pacific Conference on Structural Engineering and Construction, Paper No. 1066
45. Kim SH, Cho KI, Choi MS, Lim JY. Development of human body model for the dynamic analysis of footbridges under pedestrian induced excitation. Steel Struct. 2008;8:333–45.
46. ISO 5982.
47. Caprani CC, Keogh J, Archbold P, Fanning P. Characteristic vertical response of a footbridge due to crowd loading. In: EURODYN 2011 Proceedings of the 8th International Conference on Structural Dynamics, Leuven, Belgium. pp. 978–985.
48. Silva FT, Brito HMBF, Pimentel RL. Modelling of crowd load in vertical direction using biodynamic model for pedestrians crossing footbridges. Can J Civil Eng. 2013. https://doi.org/10.1139/cjce-2011-0587.

49. Toso MA, Gomes HM, da Silva FT, Pimentel RL. Experimentally fitted biodynamic models for pedestrian-structure interaction in walking situations. Mech Syst Signal Process. 2016. https://doi.org/10.1016/j.ymssp.2015.10.029.
50. Racic W, Pavic A, Brownjohn JMW. Experimental identification and analytical modelling of human walking forces: literature review. J Sound Vib. 2009. https://doi.org/10.1016/j.jsv.2009.04.020.
51. Wang H, Chen J, Brownjohn JMW. Parameter identification of pedestrian's spring-mass-damper model by ground reaction force records through a particle filter approach. J Sound Vib. 2017. https://doi.org/10.1016/j.jsv.2017.09.020.
52 Ye XW, Dong CZ, Liu T. A review of machine vision-based structural health monitoring: methodologies and applications. J Sens. 2016. https://doi.org/10.1155/2016/71030-39.
53. Bocian M, Nikitas N, Kalybek M, et al. Dynamic performance verification of the Rędziński Bridge using portable camera-based vibration monitoring systems. Archiv Civ Mech Eng. 2023. https://doi.org/10.1007/s43452-022-00582-7.
54. Rothberg SJ at al., An international review of laser Doppler vibrometry: Making light work of vibration measurement, Opt. Laser Eng. 2017; https://doi.org/10.1016/j.optlaseng.2016.10.023
55. Pakos W at al., Experimental research of cable tension tuning of a scaled model of cable stayed bridge, Arch.Civ.Mech.Eng. 2016; https://doi.org/10.1016/j.acme.2015.09.001
56. The LMS Test.Lab Modal Analysis manual LMS Test.Lab
57. Ewins DJ. Modal testing: theory, practise and application. 2nd ed. Philadelphia, PA, USA: Research Studies Press Ltd.; 2000.
58 Benedettini F, Gentile C. Operational modal testing and FE model tuning of a cable-stayed bridge. Eng Struct. 2011. https://doi.org/10.1016/j.engstruct.2011.02.046.
59 Thomson W. Theory of Vibration with Applications. 4th ed. CRC Press; 2018.
60. Simulia ABAQUS. 2013. Users' Manual Version 6.13 Documentation; Dassault Systemes: Velizy-Villacoublay, France, 2015